Hierarchical Control of a Multi-building Microgrid for the Integration of Prosumers in the Electrical System

by

Mohammad Irfan Yousuf

Submitted to the Department of Electrical Engineering, Electronics, Computers and Systems
in partial fulfillment of the requirements for the degree of
Erasmus Mundus Master Course in Sustainable Transportation and Electrical Power Systems
at the

UNIVERSIDAD DE OVIEDO

September 2020

Author . . . .
Mohammad Irfan Yousuf

Certified by. . . . .
Ángel Navarro Rodríguez
Assistant Professor
Thesis Supervisor

Hierarchical Control of a Multi-building Microgrid for the Integration of Prosumers in the Electrical System

by

Mohammad Irfan Yousuf

Abstract

The hierarchical control structure of a multi-building microgrid usually contains four levels. Inner control of the converter, primary droop control, secondary control to eliminate the steady state error inherent from the primary control and tertiary control to exchange power from the microgrid to the grid and vice-versa. Advanced control strategies are essential components for understanding the microgrids to provide control over the production of power from renewable sources. This thesis reviews the status of the hierarchical control strategies applied to microgrids, proposes a control structure based on the existing methods for a case study consisting in a multi-building microgrid and discusses the future trends. Different droop control structure based on voltage levels is studied. An improved secondary control to compensate the communication delay and improve microgrid stability has been proposed in this thesis with Smith Predictor. Communication channel is modelled using Poisson distribution and impact of variable communication delay on the microgrid is also briefly studied. Tertiary control which is generally more related to economic optimization based on electricity market and energy prices has been modelled and simulated to allow the microgrid act as a single entity which can receive active and reactive power commands from the (DSO) as a dispatchable PQ node. Additionally, the coordination among different control levels is reviewed.

Thesis Supervisor: Ángel Navarro Rodríguez
Title: Assistant Professor

Acknowledgments

First of all, I want to express my sincere gratitude to my supervisor, Assistant Professor Ángel Navarro Rodríguez, for giving me a vote of confidence, for his guidance, for his patience, for his dedication, for all the knowledge he has conveyed me, for acknowledging all my efforts and for constantly supporting my motivation. Thank you for understanding and for enduring me during me difficult times and for celebrating every little achievement.

I would like to thank Laboratory for Electrical Energy Management Unified Research (LEMUR) group for offering me the opportunity to work with them in this project. Special thanks to Professor Pablo Garcia Fernandez and Professor Cristian Blanco for their valuable time and assisting me throughout my thesis. I would also thank all my professors from Sapienza University of Rome, University of Nottingham and University of Oviedo. Special mentions to Mhret Berhe Gebremariam and Hafte Hayelom Adhena for supporting me during the thesis.

This thesis would not have been possible without the support of the EMJMD STEPS consortium. The STEPS journey has been a life changing experience for me. It has certainly shaped my thinking ability for better and broaden by creative horizon. From group study to working on complex projects with colleagues from different parts of the world makes this program truly international. These two remarkable years would not have been as smooth as it was had there not been Siam Hasan Khan, Sabbir Ahmad, Nahid Nasrin and Syed Asim Ali Shah. Thank you all for tolerating me and I will forever miss our time spend together in Italy, United Kingdom and Spain.

None of this would have been possible without the will of Allah (SWT), on the one hand, and the blessings of my dear parents, Md. Iqbal Yousuf and Amina Khatun,and my sister Afsara Tasnim, on the other, who have always prayed for my success.

Contents

List of Figures

List of Tables

Acronyms

AC Alternating Current.

B2B Building to Building.

DC Direct Current.

DER Distributed Energy Resource.

DG Distributed Generation.

DHEMS Dynamic Hybrid Energy Management System.

DSO Distribution system Operator.

HV High Voltage.

LV Low Voltage.

MG Microgrid.

MGCC Microgrid Central Controller.

PCC Point of Common Coupling.

PI Proportional Integral (Controller).

PV Photovoltaic.

Nomenclature

δ_{grid} Phase of GRID

δ_{mg} Phase of MG

Δf Frequency Control Signal from Secondary Control to Buildings

ΔV Voltage Control Signal from Secondary Control to Buildings

C_P Active Power Droop Coefficient

C_Q Reactive Power Droop Coeffient

f_n Nominal Frequency

f_{mg}^{pcc} Frequency of MG at PCC

f_{mg}^{ref} Reference Frequency of MG

$G_d(s)$ Transfer Function of Delay

$G_{f\ sec}(s)$ Transfer Function of Secondary Frequency Controller

G_{if} Secondary Control Integral Gain for Frequency Control

G_{iP} Tertiary Control Integral Gain for Active Power Control

G_{iv} Secondary Control Integral Gain for Voltage Control

G_{pf} Secondary Control Proportional Gain for Frequency Control

G_{pP} Tertiary Control Proportional Gain for Active Power Control

G_{pQ} Tertiary Control Integral Gain for Reactive Power Control

G_{pQ} Tertiary Control Proportional Gain for Reactive Power Control

G_{pv} Secondary Control Proportional Gain for Voltage Control

$G_{v\,\mathrm{sec}}(s)$ Transfer Function of Secondary Voltage Controller

L_{grid} Grid Inductance

L_{Line} Line Inductance

P_0 Nominal Active Power

P_{max} Maximum Active Power

P_{pcc} Active Power at PCC

P_{pcc}^{ref} Active Power Reference at PCC

Q_0 Nominal Reactive Power

Q_{max} Maximum Reactive Power

Q_{pcc} Reactive Power at PCC

Q_{pcc}^{ref} Reactive Power Reference at PCC

R_{grid} Grid Resistance

R_{Line} Line Resistance

T_{delay} Communication Delay

V_n Nominal Voltage

$V_{mg}^{\,pcc}$ Voltage of MG at PCC

$V_{mg}^{\,ref}$ Reference Voltage of MG

Chapter 1

Thesis Introduction

1.1 Introduction

Renewables energy are the main sources that can be integrated into the network in the form of Distributed Generators (DGs) or Microgrids (MGs)[8]. Environmental impacts, economic concerns, and the increasing integration of small-scale renewable sources are all making the centralized power generation concept outdated and moving towards a more distributed future[9][10][11][4]. The microgrid concept acts as a bridge between the HV transmission and LV distributed generation. MGs are LV electrical distribution systems, composed of DG, energy storage, and load. MGs can connect to a large power system via PCC, but they can also operation in 'island' mode independent of the main grid. Island operation of microgrids could be planned or could happen instantly if a fault detected requires disconnection of the MG from the main grid.

Energy generation from MG can be a mixture of PV, wind, etc. Renewable energy sources (RES) either generates DC power or variable-frequency AC power and are linked with a synchronous AC grid through power electronic inverters. These inverters are responsible for the cooperation, power balance and load sharing in the network. The control approach can be centralized as well as decentralized and have aimed to tackle these tests and have then been grouped into a hierarchical control architecture[12].

The control hierarchy usually contains four levels. The first one is the inner control loop of the inverter. Second one is the primary control, responsible for stabilizing the microgrid and achieve power sharing[13]. Secondary control removes the deviation in both voltage and frequency[14]. The final tertiary control is concerned with global economic dispatch over the network and depends on current energy markets and prices.

This thesis reviews all the levels except the inner control level of the inverter, considering the inverters as ideal voltage sources. A new improved secondary control scheme is proposed, communication channel is studied and finally a tertiary control level is included to allow the exchange of active and reactive power with the grid. The proposals and models presented in this thesis are supported with simulations results using Matlab/Simulink®.

1.2   Motivation

The green house gas emission from traditional centralized power generation rises concerns about the environmental effect[15]. To combat this situation, modern power system is moving towards decentralized renewable power generations, like wind and PV. These renewable sources allow consumers to become prosumers; they can generate as well as sell electricity. Prosumer communities aim to transform traditional consumers to become active prosumers. Thus, improving the efficiency of the microgrid and offering economic, operational, and environmental benefits. Integrating active buildings (prosumers) in the main grid and exchange of power between multi-building microgrid and main grid requires hierarchical control. Any integration of distributed generation or load demand by prosumers should not affect the grid quality and stability and should not deviate voltage and frequency of the system beyond the desired operating conditions. Hierarchical control aims to control voltage and frequency within the microgrid, and power exchange between the different components of the microgrid and the main grid, in order to keep microgrid devices, like household appliances, safe of any damage created by sudden change in MG demand or genera-

tion. In a hierarchical control, primary droop control mimics the primary control of synchronous generators seen in conventional grid and limits any change any change in voltage and frequency. Secondary control acts to get the voltage and frequency to nominal value, eliminating the steady state errors implicit in the primary droop control. and tertiary control allows power exchange between MG and main grid. For all these reasons this thesis is going to explore the hierarchical control used in microgrids for enabling a proper integration of prosumers in the grid.

1.3   Thesis objectives

The main objective of this master thesis is developing the hierarchical control of a multi-building microgrid.

1. Study of the state of art regarding hierarchical control and analyzing the actual trends in order to implement in simulations a hierarchical control in a case of study consisting of a microgrid with 2 prosumer buildings and a single conventional building.

2. Representation of the active building with a grid-supporting converter.

3. Modelling and analysis of the communication link required for a centralized secondary controller.

4. Improvement in microgrid stability by using Smith Predictor to compensate for the communication delay.

5. Verifying the system with variable communication delay (modelled using Poisson Distribution).

6. Implementation of tertiary controller to exchange power from the microgrid to the main grid.

7. All simulations are performed in MATLAB/Simulink®.

1.4   Thesis structure

In this master's thesis, chapter 2 presents the ongoing research on the topic by various other universities around the world. This chapters also represents all the theory needed to understand the multi-building microgrid hierarchical control. In summary, this chapter gives a brief discussion on grid-forming converter and its equivalent model to be used to represent building in the thesis, primary droop control, secondary control, and tertiary control. Apart from that it also discusses the Smith Predictor theory to be used in Chapter 4 to improve the existing secondary control method. In the later chapter, control block diagrams from this chapter is used to simulate and verify the results.

Chapter 3 presents and explains a block diagram of the studied microgrid. It also explains the location and function of the different control layer in the microgrid.

Chapter 4 shows the methodology used to make a simplified model of the secondary controller and improve the system stability and response of the secondary control compared to traditional secondary control using Smith Predictor. In this chapter, performance of the secondary control in tested in both island and grid connected mode.

Chapter 5 models the communication delay using poison distribution and tests its effects on the systems already developed in chapter 4. This chapter also considers what may happen in case of communication failure and assesses what happens to system stability if the Smith Predictor already know the communication delay randomness.

Chapter 6 develops the simplified model for finding the control gain value range of the tertiary control and uses those values to simulate the overall microgrid. It also highlights possible methods to that can be adapted to improve the system response.

Chapter 7 includes the conclusions and the possible future lines derived from this thesis.

Chapter 2

State of the Art

This chapter covers the theory and methodology used to implementing the hierarchical multi-building microgrid control.

2.1 Discussion about hierarchical microgrids control structure

Hierarchical control structures are important to proper control of MGs for providing stability and efficient operation[14]. The essential roles that can be achieved using these control structures are voltage and frequency regulation, active and reactive power control between multi-building microgrid with the main grid.

In such hierarchical approach four control levels have been defined. Inner control loop of the interlinking converter make it work like VSG or grid-forming based converter. The primary control level, which is independent and deals with the inner control loop of the each building to provide voltage and frequency stabilization. Conventionally, active power – frequency droop control and reactive power-voltage droop are adopted. Although the primary level does not require communication, to achieve global controllability of the MG, secondary control is used[10].

The conventional secondary control approach uses an MG central controller (MGCC), which includes a slow control loop to measure voltage and frequency at PCC and

send back the control output information to each building via communication channel. This MGCC also houses tertiary control, which is more related to economic optimization, based on energy prices and electricity markets. Tertiary control exchanges information with the distribution system operator (DSO) to make viable and to optimize the multi-building MG operation within the utility grid[16][17].

Secondary control is envisioned to compensate voltage and frequency deviations produced inside building local primary control. For decades, this concept has been in use in large utility power systems to control frequency of a large-area electrical network, and now it has been applied to MGs to restore frequency and voltage deviations[18][19]. Fig 2-1 highlights the duties assigned to each control layer for efficient multi-building operation.
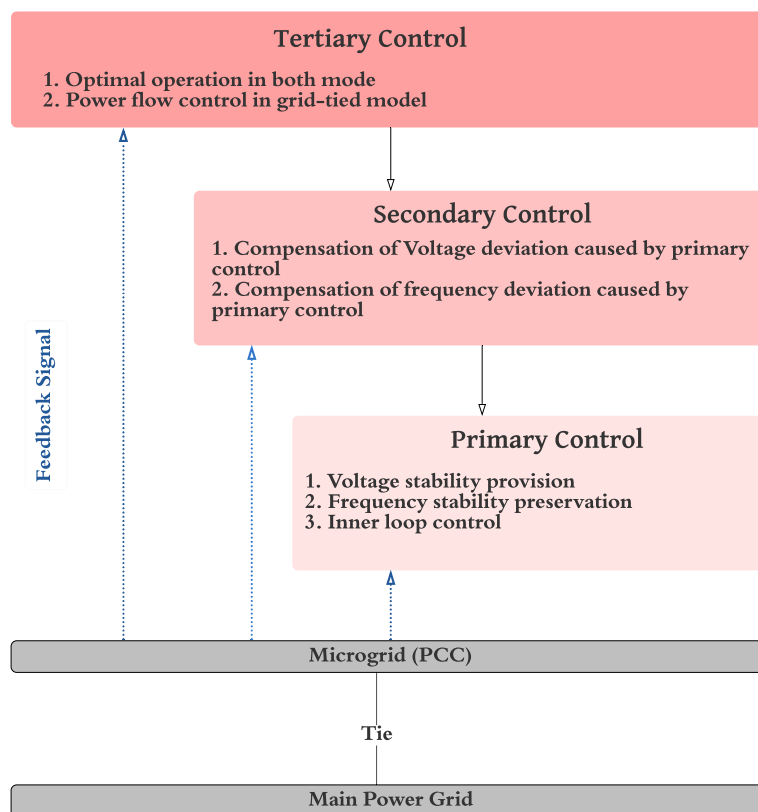
Figure 2-1: Hierarchical control levels of a microgrid[1].

2.2 Classification of power converters in AC microgrids
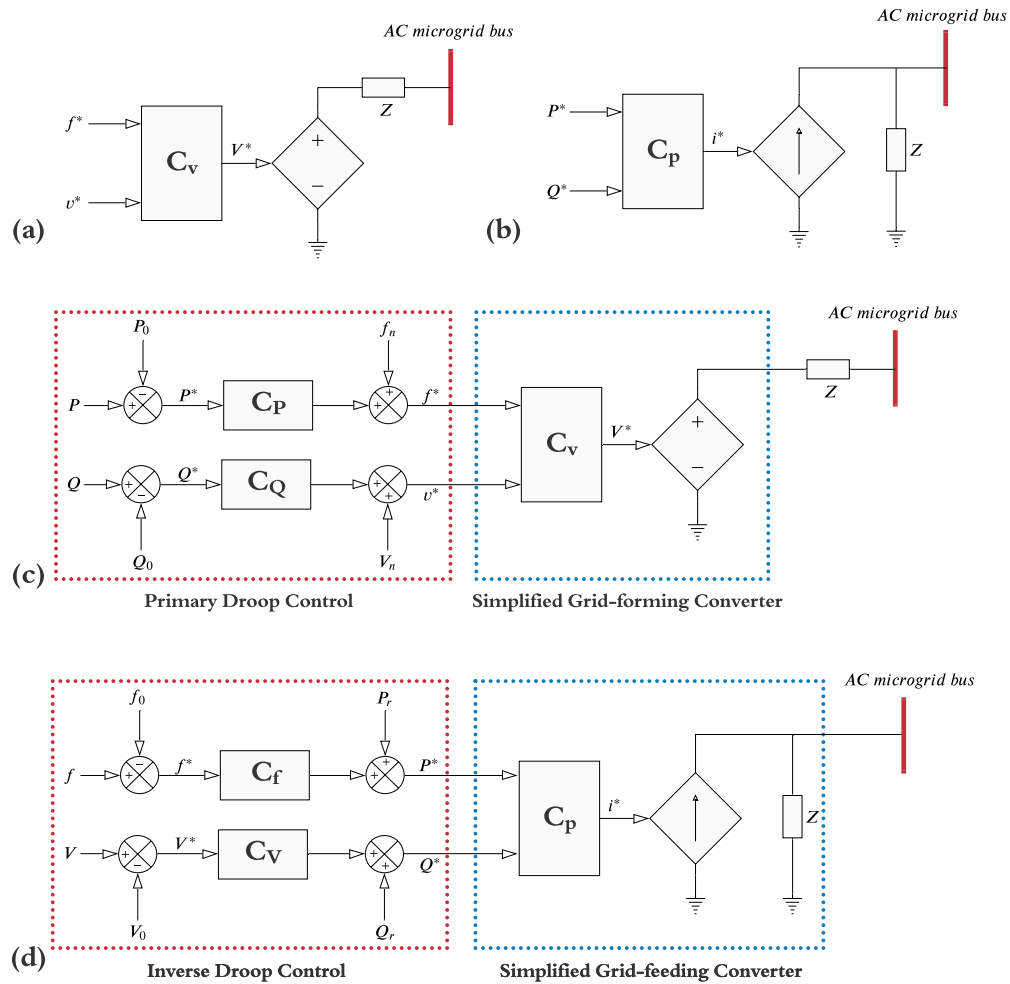
Figure 2-2: Simplified representation of grid-connected power converters, (a) grid-forming, (b) grid-feeding, (c) voltage-source-based grid-supporting, and (d) current-source-based grid-supporting[2].

Depending of the operation of the converter in ac microgrid, they can be sorted into grid-feeding, grid-supporting and grid-forming power converters. Grid-forming converters can be represented as an ideal ac voltage source with a low output impedance, setting the voltage amplitude v^* and frequency f^* of the local grid by using a proper control loop shown in Fig 2-2(a).

Whereas grid-feeding converters are mainly designed to deliver power to an energized power grid. They are represented by an ideal current source connected to the

Table 2.1: Typical Line Impedance Values

Type of Line	R(ohm/km)	X(ohm/km)	R/X(p.u)
Low Voltage Line	0.642	0.083	7.7
Medium Voltage Line	0.161	0.190	0.85
High Voltage Line	0.06	0.191	0.31

grid in parallel with high impedance. A simplified scheme is of grid-feeding converter is shown in Fig 2-2(b), where P* and Q*. It is important to remember that this current source should be perfectly synchronized with the ac voltage at the connection point, to regulate accurately the active and reactive power exchanged with grid.

Lastly, the grid-supporting converters are represented either as an ideal ac-controlled voltage source or ac-controlled current source, as shown in Fig 2-2(c) and (d), respectively. These converters control the output voltage/current to the value of the grid frequency and voltage close to their rated values. A grid-feeding needs a generator or a power converter to form the grid voltage to be able to operate. Therefore, this kind of converter cannot operate independently in island mode. On the other hand, a grid-forming power converter usually operates specifically in islanded mode, since in the main grid the ac voltage is conventionally formed by synchronous generators [2].

A grid-supporting power converter is in between a grid-feeding and a grid-forming power converter, being its main objective to deliver proper values of active and reactive power to contribute to the regulation of the grid frequency and the voltage.

For this master's thesis, grid-forming based grid-supporting structure as shown in Fig 2-2(c) is chosen to represent the generation at building level as it can operate in both grid-connected and islanded mode, as a synchronous generator does in a conventional grid. It is a controlled voltage source with link impedance. Grid-feeding based grid-supporting structure is not as it needs one grid former to operate.

26
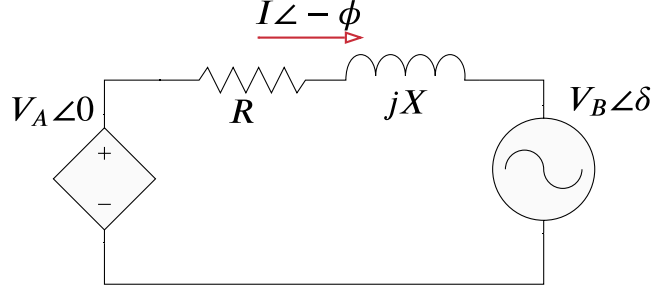
Figure 2-3: Equivalent circuit modeling of a power converter connected to a distribution network[2].

2.3 Primary control in MGs based on droop control and grid-supporting converters

The droop control methods are implemented in grid-supporting power converters to regulate the exchange of active and reactive powers with the grid, to keep the grid frequency and voltage amplitude under control. The core idea to support the droop control comes from mimicking the self-regulation capability of the synchronous generator in grid-connection mode. Lowering the active power sent when the grid frequency increases and decreasing the injected reactive power when the grid voltage amplitude jumps up.

Taking into account that the power converter as an ideal controllable voltage source that is connected to the mains through a given line impedance as shown in Fig A.1, the active and reactive powers that it will deliver to the grid can be written as:

$$P_A = \frac{V_A}{R^2 + X^2} \left[R \left(V_A - V_B \cos \delta \right) + X V_B \sin \delta \right] \tag{2.1}$$

$$Q_A = \frac{V_A}{R^2 + X^2} \left[X \left(V_A - V_B \cos \delta \right) - R V_B \sin \delta \right] \tag{2.2}$$

where P_A and Q_A are the active and reactive powers, respectively, flowing from the source A (power converter) to the B (grid), V_A and V_B are the voltage values of these sources, δ corresponds to the phase-angle difference between the two voltages, $Z = R + jX$ is the interconnection line impedance and θ is the impedance angle.

27

2.3.1 Influence of grid impedance : inductive line

The inductive component of the line impedance in HV and MV networks is typically much higher than the resistive one, as shown in Table 2.1 [2].
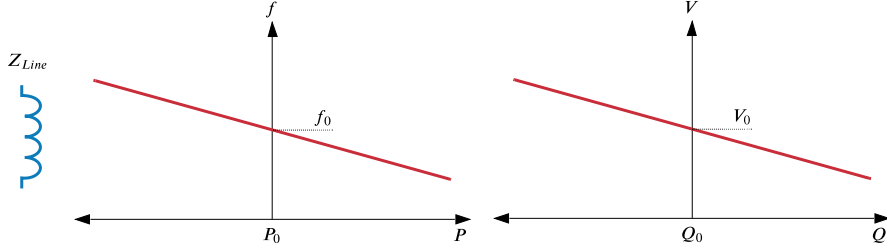
Figure 2-4: Frequency and voltage droop characteristics in inductive grid[3]

Therefore, the resistive part can be neglected without making any significant error. In addition, the power angle δ in such lines is small, so it can be assumed that $\sin \delta \approx \delta$ and $cos(\delta) \approx 1$ [20][21][22]. Therefore, 2.1 and 2.2 can be rewritten as:

$$P_A \approx \frac{V_A}{X} \left(V_B \sin \delta\right) \Rightarrow \ \delta \ = \frac{X P_A}{V_A V_B} \tag{2.3}$$

$$Q_A \approx \frac{V_A}{X} \left(V_A - V_B \cos \delta\right) \ \Rightarrow \ V_A - V_B \ = \frac{X Q_A}{V_A} \tag{2.4}$$

Expressions 2.3 and 2.4 show a direct relationship between the power angle δ and the active power P, as well as between the voltage difference $V_A - V_B$ and the reactive power Q. These relationships permit regulating the grid frequency and voltage at the point of connection of the power converter, by controlling the value of the active and reactive powers delivered to the grid[3]. Therefore, the following droop control expressions can be written for inductive lines:

$$f - f_0 \ = -C_P \left(P - P_0\right) \tag{2.5}$$

$$V - V_0 \ = -C_Q \left(Q - Q_0\right) \tag{2.6}$$

$$C_P = \frac{-\left(f_0 - f_{\min}\right)}{P_0 - P_{\max}} \tag{2.7}$$

$$C_Q = \frac{V_{\max} - V_{\min}}{2 Q_{\max}} \tag{2.8}$$

28

where $f - f_0$ and $V - V_0$ represent the grid frequency and the voltage deviations, respectively, from their rated values, and $P - P_O$ and $Q - Q_O$ are the variations in the active and reactive powers delivered by the power converter to compensate such deviations. These relationships can be graphically represented by the droop characteristics shown in Fig 2-4, where, as stated in equations 2.5 and 2.6, the gain of the control action in each case, i.e., the slope of the frequency and voltage droop characteristic, is set by the C_P and C_Q parameters, respectively. C_P and C_Q gain values are calculated with the equations given in 2.7 and 2.8. Therefore, as depicted in Fig 2-4, each of the grid-supporting power converters operating in a microgrid will adjust its active and reactive power reference according to its P/f and Q/V droop characteristic to participate in the regulation of the microgrid frequency and voltage, respectively[23][24].

2.3.2   Influence of grid impedance : resistive line

Contrary to the case of HV networks, the grid impedance in LV networks is mainly resistive, as it is shown in Table I [46], and thus, the inductive part can be neglected. As a consequence, and maintaining the assumption that the power angle δ has a small value, 2.1 and 2.2 give rise to:

$$P_A \approx \frac{V_A}{X} (V_A - V_B \cos \delta) \;\Rightarrow\; V_A - V_B \;=\; \frac{RP_A}{V_A} \tag{2.9}$$

$$Q_A \approx -\frac{V_A V_B}{R} (\sin \delta) \Rightarrow\; \delta \;=\; -\frac{RQ_A}{V_A V_B} \tag{2.10}$$

Therefore, the voltage amplitude in LV networks depends mainly on the active power flow, while their frequency is mainly affected by the reactive power injection. From 2.9 and 2.10, the following droop control expressions can be written for resistive lines:

$$V - V_0 \;=\; -C_P (P - P_0) \tag{2.11}$$

$$f - f_0 \;=\; -C_Q (Q - Q_0) \tag{2.12}$$

being their droop characteristics represented in Fig [48], [49], which depicts the P/V and the Q/f droop control actions to be taken in resistive networks for regulating the grid voltage and frequency.
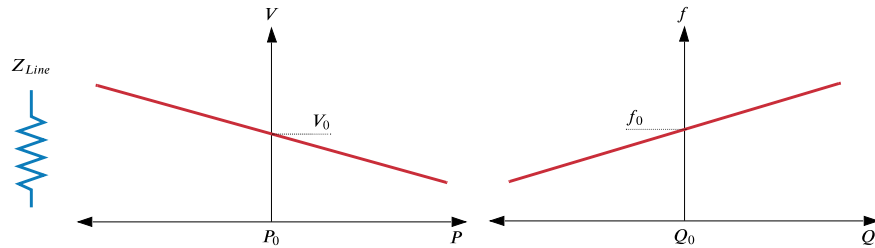
Figure 2-5: Voltage and frequency droop characteristics (resistive grids) generally in LV systems[2]

For the purpose of this thesis, inductive droop is implemented, the characteristics of which is shown in Fig 2-4. Appendex A and B lists all the parameters used in simulations and simulink figures respectively.

2.3.3 Grid-forming power converters

The grid supporting converter be a combination of a droop control and a grid-forming that operates as a voltage source with adjustable frequency and voltage magnitude. As voltage sources, they present a low-output impedance, so they need an extremely accurate synchronization system to operate in parallel with other grid-forming converters. Power sharing among grid-forming converters connected in parallel is a function of the value of their output impedances. A practical example of a grid-forming power converter can be a standby UPS. This system remains disconnected from the main grid when the operating conditions are within certain limits. In the case of a grid failure, the power converter of the UPS forms the grid voltage. In a microgrid, the ac voltage generated by the grid-forming power converter will be used as a reference for the rest of grid-feeding power converters connected to it. Fig 2-6 shows an example of a controller for a grid-forming power converter, which is implemented by using two cascaded synchronous controllers working on the dq reference frame. The inputs to the control system are the amplitude V and the frequency of the voltage

30

to be formed by the power converter at the point of common coupling (PCC)[25][26]. The external loop controls the grid voltage to match its reference value, while the internal control loop regulates the current supplied by the converter. Therefore, the controlled current flowing though the inductor L_F charges the capacitor C_F to keep the output voltage close to the reference provided to the voltage control loop. Usually, in industrial applications, these power converters are fed by stable dc voltage sources driven by batteries, fuel cells, or another primary source.

Figure 2-6: Basic control structure in a three-phase grid-forming voltage source inverter generating a sinusoidal voltage determined by a nominal voltage amplitude v^* and reference frequency ω^*[2].

In the following chapters, these cascaded voltage and current loops are called inner loop control in the block diagram and for the case of running the simulation faster, instead of using Fig 2-6, Fig 2-2(a) is used to simulate the hierarchical control level of multi-building microgrid. So, Fig 2-2(c) represent a building in the simulation of the thesis. Primary Droop Control structure is discussed in the following subsection.

2.4 Secondary control of microgrid

The task of second control is to supervise and monitor the system, to regulate for deviations in both voltage and frequency towards zero following every change in load or generation in the MG [27]. Fig 2-7 shows both the primary and secondary control action. It helps power systems by correcting grid frequency deviations within tolerable range—for example by $\pm 0.1 Hz$ in Nordel (North of Europe) or $\pm 0.2 Hz$ in UCTE (Continental Europe)[5]. The principle of the secondary control in MGs is shown in Fig 2-8. In practice, the secondary control has slower dynamic response to variation, as compared to primary control level. This control level can be divided into centralized and decentralized control. Most of the research on MG control has been performed by Chandorkar et al.[28] and Guerrero et al.[7]. For this master's thesis we are considering centralized architecture only.
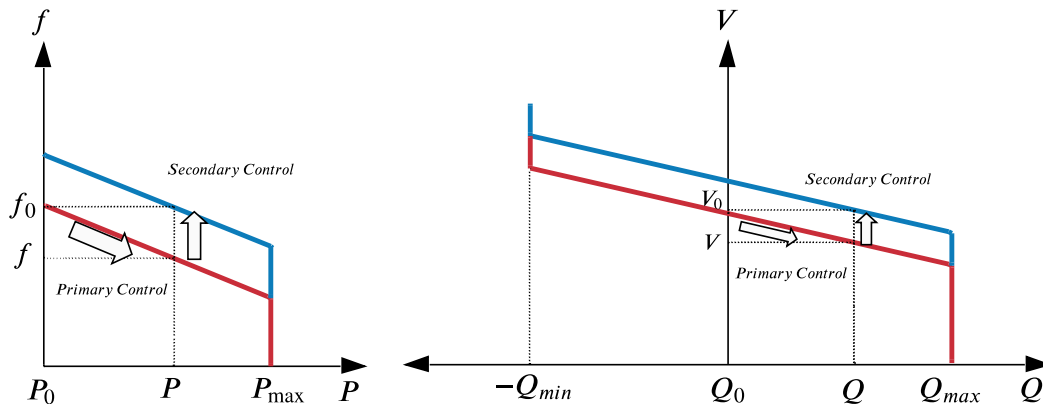
Figure 2-7: $P - f$ and $Q - V$ primary and secondary control response[4].

2.5 Centralized secondary control architecture of MGs

In this technique, the central controller allows each building to generate or absorb the required active or reactive power to control of the PCC frequency and voltage. The control structure of centralized secondary control is shown in Fig 2-9. The outputs of the centralized secondary control are added to the primary droop control reference
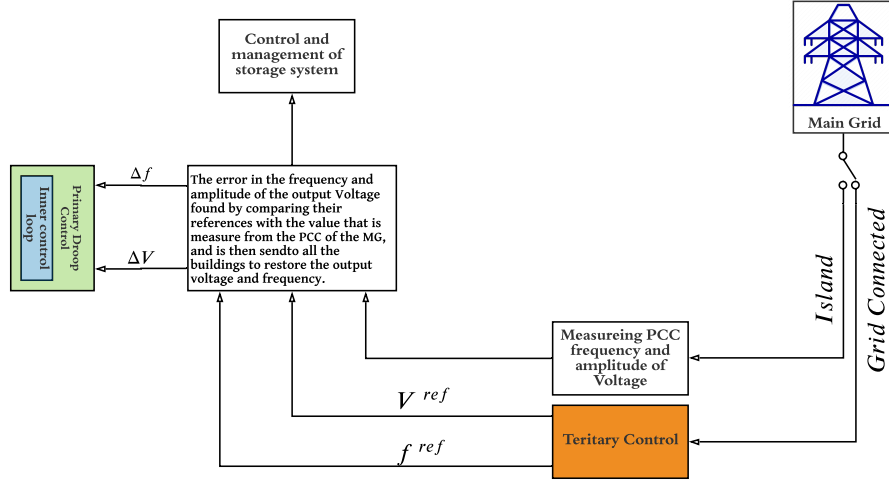
Figure 2-8: Principle of the secondary control in Microgrids[5].

through a communications link to generate the reference voltage and frequency for the controlled voltage source.

2.5.1 Secondary frequency control

Conventionally, secondary controllers for large power systems are based on frequency restoration, since the frequency of the generator-dominated grids is highly dependent on the active power. Control variable frequency provides information related to the consumption/generation balance of the grid.

Similar concept has been implemented in order to restore the frequency of $P - f$ droop controlled MG. The frequency restoration compensator can be derived as follows:

$$\Delta f = G_{pf} \ \left(f \ _{mg}^{ref} - f \ _{mg}^{pcc}\right) + G_{if} \ \int \left(f \ _{mg}^{ref} - f \ _{mg}^{pcc}\right) \tag{2.13}$$

with G_{pf} and G_{if} being the control parameters of the secondary control PI compensator. The frequency at PCC ($f \ _{mg}^{pcc}$) are measured and compared to the references ($f \ _{mg}^{ref}$) and the errors processed through the compensators (Δf) are sent to all the buildings in order to restore the frequency of MG.
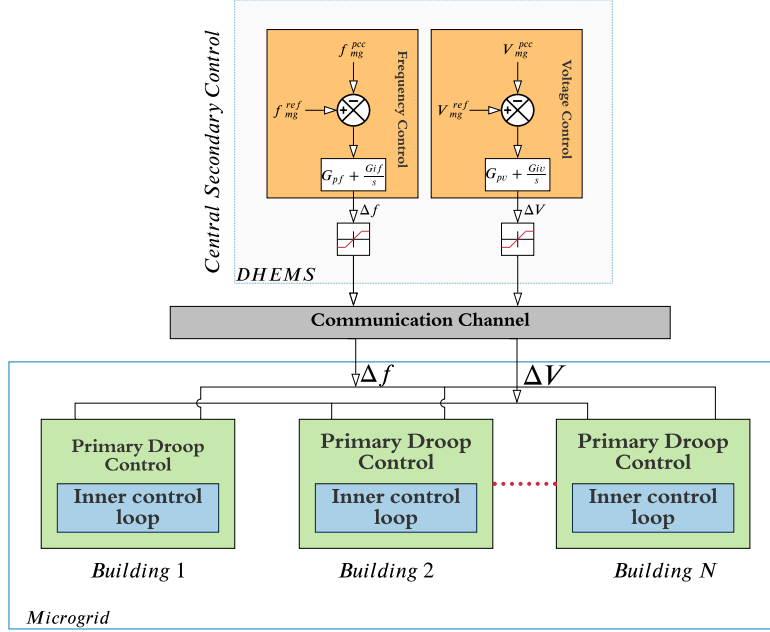
Figure 2-9: Scheme of the central secoondary control[5].

2.5.2 Secondary voltage control

The voltage is also controlled by using similar procedure as the frequency secondary control. When the voltage in the PCC of MG is out from a certain range of nominal rms values, a PI control that compensates the voltage amplitude in the MG PCC, pass the error through a dead band, and send the voltage information by using communication channel to each building. So, it can be implemented together with the frequency restoration control loop at the DHEMS. The voltage restoration control loop is derived as follows:

$$\Delta V = G_{pv}\ \left(V\,_{mg}^{ref} - V\,_{mg}^{pcc}\right) + G_{iv}\ \int \left(V\,_{mg}^{ref} - V\,_{mg}^{pcc}\right) \tag{2.14}$$

with G_{pv} and G_{iv} being the PI controller parameters of the voltage secondary control. The voltage at PCC ($V\,_{mg}^{pcc}$) are measured and compared to the references ($V\,_{mg}^{ref}$) and the control signal (ΔV) is sent to the primary control level of each building in order to remove the steady-state errors produced by droop control. The secondary control structure shown in Fig 2-9 is modified into a simplified model covered in chapter 4 and

another improved secondary control model is suggested by the implementing Smith Predictor to compensate for the communication delay which impacts stability of the system. Chapter 2.6 covers the basics of Smith Predictor.

2.6 Smith Predictor to compensate the communication delay in secondary control

2.6.1 Introduction to Smith Predictor

Time delay reduces system stability, so it is important to compensate the effect of the delay for improving system stability[29]. One of the mathematical models for capturing the structure of delay component in a control system is the Smith Predictor[30]. Smith Predictor not only brilliantly depicts the structure of delay component, but also gives an intuitive explanation about the compensation process.

Delay can be caused by transportation and communication lag, time for generating feedback in a sensor system that requires sampling and analysis, time to generate control signal, and system parameters approximation using lower order. Delays always reduce stability of minimum phase systems (systems that do not have poles or zeros in the right-hand side of s-plane or do not have other delay component), so that it is important to analyze system stability under the presence of delays[31].Delay in a control system is usually described in the complex frequency domain. Fig 2-10 shows the frequency domain delay response.

$$\xrightarrow{X_{in}(s)} \boxed{e^{-Ts}} \xrightarrow{X_{out} = X_{in}(s)e^{-Ts}}$$

Figure 2-10: Delay in the frequency domain[6]

2.6.2   Smith predictor general structure

Smith Predictor is a delay compensation method commonly used in control systems. This technique is used for both small and large delay. Smith Predictor basically removes the delay component from the system's closed loop. Delay in the system's close loop can affect system stability. So, removing delay from the loop improves system stability[32].
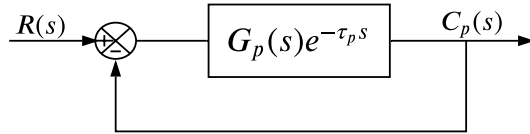
Figure 2-11: Closed loop control system with delay[6]

Fig 2-11 shows a control system with delay inside its closed loop. To remove the delay component from the closed loop a compensator C*(s) can be added as shown in Fig 2-12.
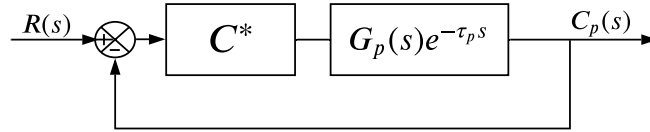
Figure 2-12: Compensator added to the system[6]

Fig 2-13 shows the structure of control system after the addition of compensator C*(s).
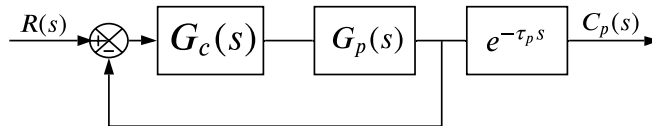
Figure 2-13: Updated structure of the system due to the addition of compensator C*(s)[6]

As system in Fig 2-12 and Fig 2-13 is equivalent, C*(s) can be found by

36

$$\frac{C^*(s)G_p\left(s\right)e^{-\tau_p s}}{1+C^*(s)G_p\left(s\right)e^{-\tau_p s}} = \frac{G_c\left(s\right)G_P\left(s\right)}{1+G_c\left(s\right)G_P\left(s\right)}e^{-\tau_p s} \tag{2.15}$$

$$C^*\left(s\right)G_p\left(s\right)e^{-\tau_p s}\left(1+G_c\left(s\right)G_p\left(s\right)\right) = G_c\left(s\right)G_p\left(s\right)e^{-\tau_p s}\left(1+C^*(s)G_p\left(s\right)e^{-\tau_p s}\right) \tag{2.16}$$

So,

$$C^*\left(s\right) = \frac{G_c\left(s\right)G_p\left(s\right)e^{-\tau_p s}}{G_p\left(s\right)e^{-\tau_p s}\left(1+G_c\left(s\right)G_p\left(s\right)\right) - G_c\left(s\right)G_p^2\left(s\right)e^{-2\tau_p s}}$$

$$\boxed{C^* = \frac{G_c\left(s\right)}{1+G_c\left(s\right)G_p\left(s\right)\left(1-\ e^{-\tau_p s}\right)}} \tag{2.17}$$

Thus, we can depict the structure of the system with Smith Predictor using 2.16.
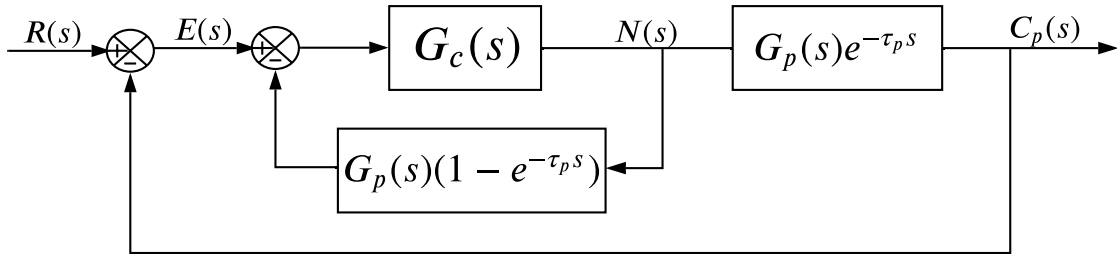
Figure 2-14: Smith Predictor general structure for delay compensation[6].

Smith Predictor structure in Fig 2-14 is the idealistic one as predictor's transfer function $G_p(s)(1-e^{-\tau_p s})$ is assumed to cancel the effect of delay in the loop perfectly.

This is explained in the following equations.

$$\frac{N(s)}{E(s)} = \frac{G_c(s)}{1 + G_c(s) G_p(s)(1 - e^{-\tau_p s})} \tag{2.18}$$

$$\frac{C_p(s)}{R(s)} = \frac{\frac{N(s)}{E(s)} \frac{C(s)}{N(s)}}{1 + \frac{N(s)}{E(s)} \frac{C(s)}{N(s)}} \tag{2.19}$$

$$\frac{C_p(s)}{R(s)} = \frac{\frac{G_c(s)}{1 + G_c(s) G_p(s)(1 - e^{-\tau_p s})}}{1 + \frac{G_c(s)}{1 + G_c(s) G_p(s)(1 - e^{-\tau_p s})}} \tag{2.20}$$

$$\frac{C_p(s)}{R(s)} = \frac{\frac{G_c(s)}{1 + G_c(s) G_p(s)(1 - e^{-\tau_p s})}}{\frac{1 + G_c(s) G_p(s)(1 - e^{-\tau_p s}) + G_c(s) G_p(s) e^{-\tau_p s}}{1 + G_c(s) G_p(s)(1 - e^{-\tau_p s})}} \tag{2.21}$$

$$\frac{C_p(s)}{R(s)} = \frac{G_c(s) G_p(s) e^{-\tau_p s}}{1 + G_c(s) G_p(s)(1 - e^{-\tau_p s}) + G_c(s) G_p(s) e^{-\tau_p s}} \tag{2.22}$$

$$\frac{C_p(s)}{R(s)} = \frac{G_c(s) G_p(s) e^{-\tau_p s}}{1 + G_c(s) G_p(s)} \tag{2.23}$$

Eq 2.23 describes the system in Fig 2-13, i.e., the expected system structure after the compensator added.

The delay compensation shown in Fig 2-13 needs a perfect estimation about process transfer function $(G_p(s)e^{-t_p s})$ which is not possible. To implement Smith Predictor in real world scenario, one must estimate G_p and $e^{-\tau_p s}$ values. If we denote the estimates to be $G_m(s)$ and $e^{-\tau_m s}$, then the Smith Predictor structure can be depicted as the following. Smith Predictor transfer function in Fig 2-14 can be obtained as
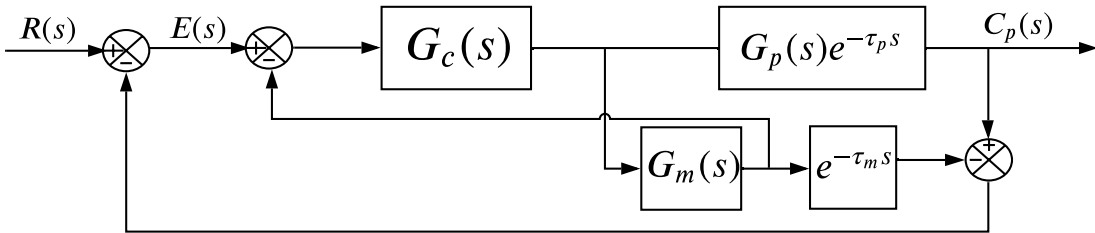
Figure 2-15: Smith Predictor with process parameter estimation[6].

follows.

$$\frac{C_p\left(s\right)}{R\left(s\right)} = \frac{\frac{G_c(s)G_p(s)e^{-\tau_p s}}{1+G_c(s)G_m(s)(1-e^{-\tau_m s})}}{1 + \frac{G_c(s)G_p(s)e^{-\tau_p s}}{1+G_c(s)G_m(s)(1-e^{-\tau_m s})}} \tag{2.24}$$

$$\boxed{\frac{C_p\left(s\right)}{R\left(s\right)} = \frac{G_c\left(s\right)G_p\left(s\right)e^{-\tau_p s}}{1 + G_c\left(s\right)G_m\left(s\right) + G_c\left(s\right)\left(G_p\left(s\right)e^{-\tau_p s} - G_m\left(s\right)e^{-\tau_m s}\right)}} \tag{2.25}$$

Eq 2.23 shows that if process parameter can be modeled without error then system transfer function in Fig 2-15 is equivalent to the system transfer function in Fig 2-13.

The model shown in Fig 2-15 is used to compensate the communication delay in the proposed secondary control of microgrid. It is covered in chapter 3.2.

2.7 Tertiary control

The aim of the tertiary control level is to manage power flow by controlling the voltage amplitude and frequency when the MG is in grid-connected mode. By measuring the active and reactive power at the PCC, and comparing it against desired reference active and reactive power to be delivered to or absorb from main grid.The frequency and voltage reference defined in 2.26 and 2.27 are used for 2.13 and 2.14 in secondary control.

$$f^{\;ref}_{\;mg} = G_{pP}\left(P^{\;ref}_{\;pcc} - P_{\;pcc}\right) + G_{iP}\int\left(P^{\;ref}_{\;pcc} - P_{\;pcc}\right) \tag{2.26}$$

$$V^{\;ref}_{\;mg} = G_{pQ}\left(Q^{\;ref}_{\;pcc} - Q_{\;pcc}\right) + G_{iQ}\int\left(Q^{\;ref}_{\;pcc} - Q_{\;pcc}\right) \tag{2.27}$$

Tertiary control is the final and slowest. Fig 2-16 shows a block diagram of Hierical control of MG including tertiary control, which is a control layer above secondary shown in Fig 2-9. Tertiary control involves the optimal operation of the MG in the economic part as well as the technical part. The tertiary control provides an economically optimal operation through grid forming supporting converters or by using a gossiping algorithm, as discussed in [1]. Technically, if a fault or any non-plane islanding issue arises for the MG, the tertiary control attempts to absorb P

from the grid such that, if the grid is not present, the frequency will start decreasing. When the expected value is surpassed, the MG is disconnected from the grid for safety, and the tertiary control is disabled [2].

In Chapter 5, a simplied model is used to find PI gains and those values are used in the tertiary controls of the original system.

Main Grid

Grid Connected

PCC

P and Q measurement from PCC

Tertiary Control

P_{pcc}

Q_{pcc}

P_{pcc}^{ref}

Q_{pcc}^{ref}

$G_{pP} + \frac{GiP}{s}$

$G_{pQ} + \frac{GiQ}{s}$

Central Secondary Control

f_{mg}^{ref}

Frequency Control

V_{mg}^{ref}

Voltage Control

f_{mg}^{pcc}

V_{mg}^{pcc}

$G_{pf} + \frac{Gif}{s}$

$G_{pv} + \frac{Giv}{s}$

Δf

ΔV

DHEMS

Communication Channel

Δf

ΔV

Primary Droop Control

Inner control loop

Primary Droop Control

Inner control loop

Primary Droop Control

Inner control loop

Building 1

Building 2

Building N

Microgrid

Figure 2-16: Hierarchical control structure of the MG[5].

41

Chapter 3

Microgrid Under Study

This chapter introduces the multi-building microgrid system under study. It explains the structure and components of the microgrid, and the location of the different control layers in the overall system.

3.1 Microgrid description

The Microgrid under study is a 3 phase 4 wire distribution network but for the purpose of this thesis we considered a balanced system, ie, neutral wire is left out. 3 phase 4 wire is generally used in LV distribution network as single phase power can be supplied to buildings as it has neutral wire. In the Fig 3-2 building 1 and 2 are prosumers (meaning the buildings has load and generation) but building 3 is conventional building, ie, does not present generation or energy storage and is connected to the microgrid by means of a conventional electrical installation (no interlinking converter). Ideally each building has PV based system with energy storage. The loads and distributed generators present inside the building are connected to the microgrid by means of an interlinking converter operated as a grid-supporting converter. As explained in chapter 2 the building are represented as grid-supporting converter able to operate in the four quadrants (generate/absorb active and reactive power), taking into account that the building present an energy storage. The management and control of the different elements within the building (PV, ESS and appliances) is

out of the scope of this master thesis. The primary droop control and interling converter control are implemented in a local controller located inside each building. The buildings are connected to the PCC via line impedance. Table 2.1 gives information about typical line impedance values. For the purpose of this thesis inductive line is considered. The maximum rated active and reactive power of the interling converter is 100kW and 100kVAr respectively. Nominal voltage magnitude and frequecny is 326.6V and 50Hz. Chapter A lists all the parameters values used in the simulation.

3.2 Controller locations

Consumers are becoming prosumers; they can generate as well as sell electricity[33]. They can store energy in EES or sell it to other prosumers or feed to the grid when they have excess electrical energy, based on the prediction of the generation and electricity cost. This method has changed the traditional power generations. This allows prosumers to trade without any intermediate aggregators and gives them to select the type of source from which they want energy from. The proposed model for the multi-building MG is shown in Fig 3-1. Each building has PV based system, AC and DC loads, and energy storage. There is a local controller in each building which performs the droop control and controls the interlinking converter by receiving control signals from the secondary control. The exchange of energy is based on the building level generation, load demand and price of energy. The central controller sends the voltage and frequency signals to the local building level controller. It also decides whether the MG to be operated in grid-connected mode or islanded.

3.3 Transformation center

Transformation center has transformer, circuit breaker and migrogrid central controller (MGCC). The MG can operate in island and grid-connected mode. Distributed Hybrid Energy Management Systems (DHMES) is a control system based on the combination of a microcontroller and a more powerful processor, such as raspberry pi
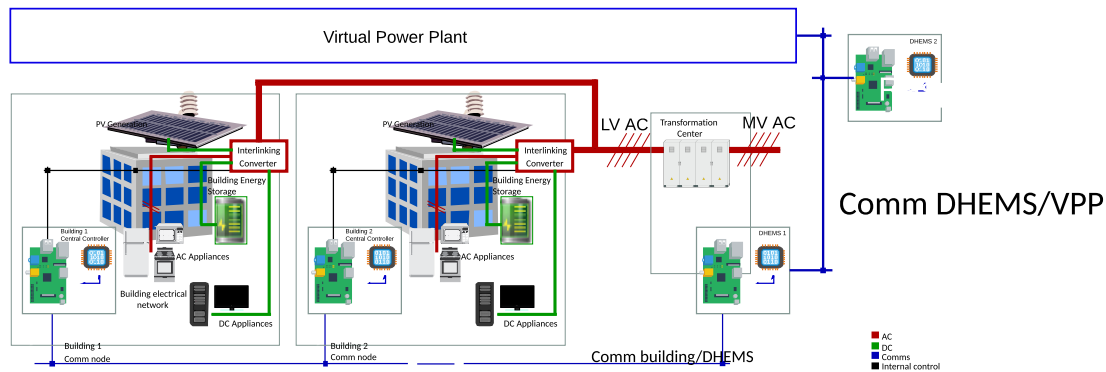
Figure 3-1: Multi-building microgrid

This image has been provided by LEMUR Group of the University of Oviedo.

or industrial PC. Fig 2-16 shows block diagram of the voltage and frequency control system inside DHEMS. The secondary controller inside DHEMS obtains real time information of voltage and frequency from the PCC and sends steady state error signal via communication channel to each building to correct any error in voltage and frequency at PCC due to change in load. The voltage and frequency at the PCC should always be maintained at the nominal operating limits. Except chapter 5, everywhere in this thesis constant communication delay of 1s is assumed. The output of the secondary controller implemented in the DHEMS is fed to the building primary control.

3.4 Exchange of active and reactive power between microgrid and main grid

In grid connected mode, another layer of control has been developed in the DHEMS, which controls the power flow from the microgrid to grid and vice-versa. It is called tertiary control shown in Fig 2-16. The tertiary control allows the multi-building microgrid to behave as a single entity that can receive commands of active and reactive power from the distribution system operator (DSO) operating as a dispatchable PQ node. Chapter 6 covers the simulation results of this control layer.
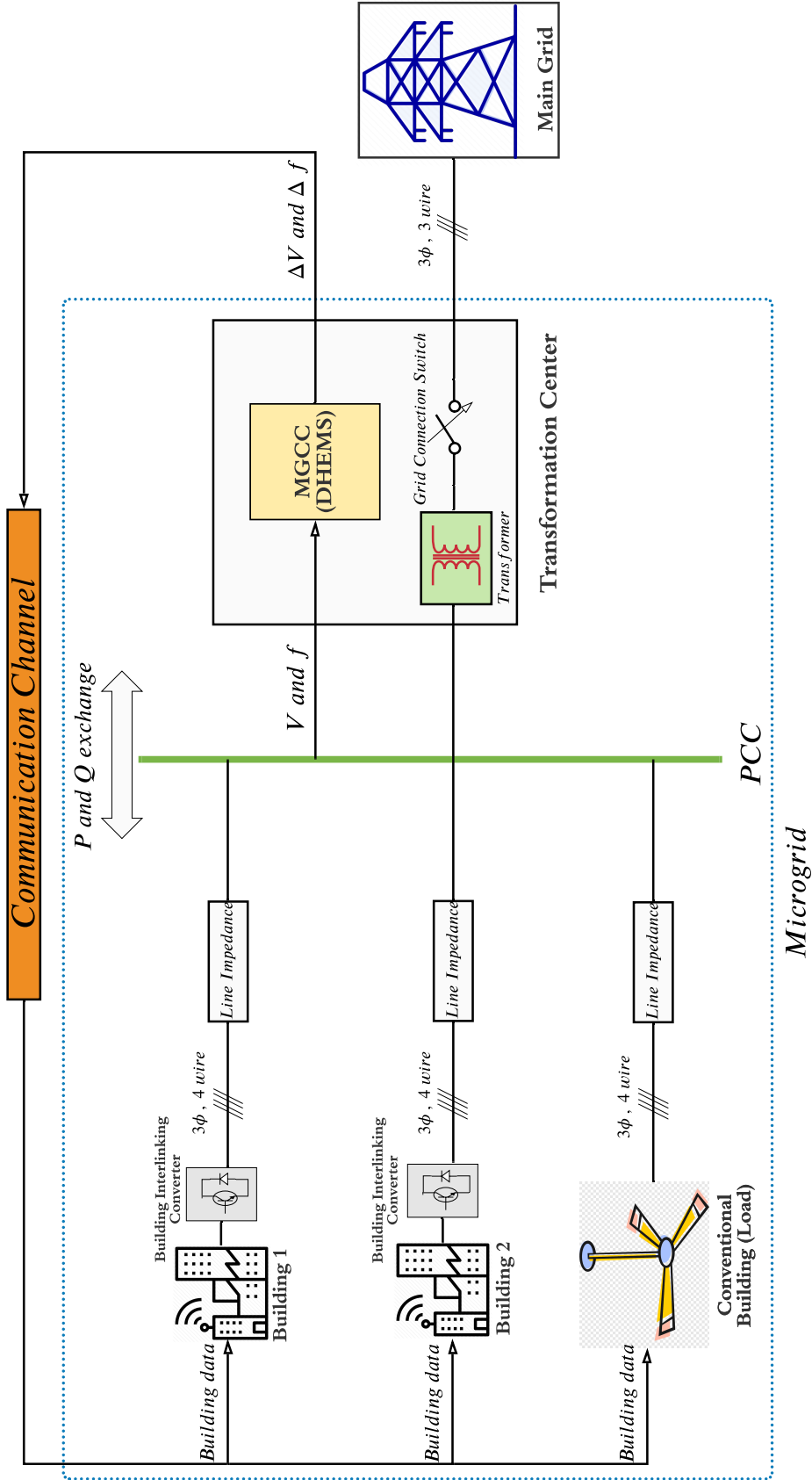
Figure 3-2: Diagram of the multi-building microgrid under study.

Chapter 4

Microgrid Primary and Secondary Control Modelling and Control Design

In this chapter, primary and secondary control of the microgrid is modelled and an improved system with Smith Predictor is also presented to compensate the communication delay implicit in centralized secondary control systems and make the system more stable as already explained in chapter 2. As shown in Fig 2-7, the purpose of primary control is to limit the change in voltage and frequency under certain change of levels and that for the secondary control is to eliminate the steady state error in frequency and voltage inherent to the primary controller. The secondary control reference to control the PCC frequency and voltage is added to the reference coming out of the primary droop controller. The output of the droop controller sets the voltage and frequency references of the building interlinking converters (or the grid-supporting converters). The internal voltage and current control loops of the interlinking converter (grid supporting converter) are neglected in this thesis, simplifying the converter model to an ideal voltage source as shown in Fig 2-2(c)). This chapter also presents the simulation results of the primary and secondary control of the microgrid described in chapter 3. The simulation parameters and figures are presented in appendix A and B respectively.

4.1 Frequency primary and secondary control model

To analyzing the system stability and to adjust the control parameters of the frequency primary and secondary control, a model has been suggested, as shown in Fig 4-1. This simplified model assumes that all buildings has the same droop control gains and neglect the line impedance. The line impedance is not included in the simplified model, but it is included in the full simulation model. Fig 4-1 includes droop control of the system (C_P), a filter to represent the PLL transfer function used to extract the frequency at PCC of MG, and the secondary control $G_f sec(s)$, followed by communication line delay $G_d(s)$.
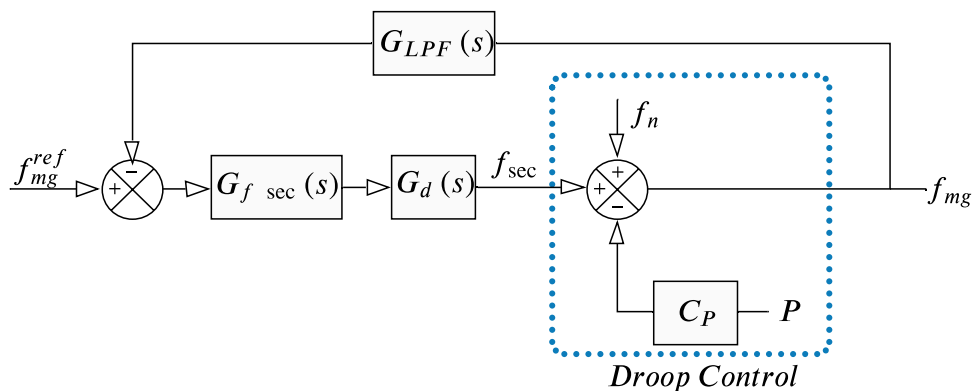
Figure 4-1: Block diagram of the simplified frequency secondary control model[7].

We can get the following model from the block diagram shown in Fig 4-1

$$f_{mg} = \frac{G_{f\ \text{sec}}(s)\, G_d(s)}{1 + G_{f\ \text{sec}}(s)\, G_d(s)\, G_{LPF}(s)} f_{mg}^{\,ref} - \frac{C_P}{1 + G_{f\ \text{sec}}(s)\, G_d(s)\, G_{LPF}(s)} P \quad (4.1)$$

Fig 4-2 shows the step response for a change in P (active power total load) from 0 to 50kW at 10s of just the primary droop control in Fig4-1 and Fig 4-3 depicts the step response of the modelled primary and secondary control in 4-1 for the same load condition. Primary control response in Fig 4-2 limits the change in frequency, but it does not bring back the system frequency back to 50 Hz, but primary and secondary control combine brings back the system frequency back to 50 Hz, shown in Fig 4-3.This model helps to adjust properly the control parameters of the secondary

48

control and to study the limitations of the communication channel delay.
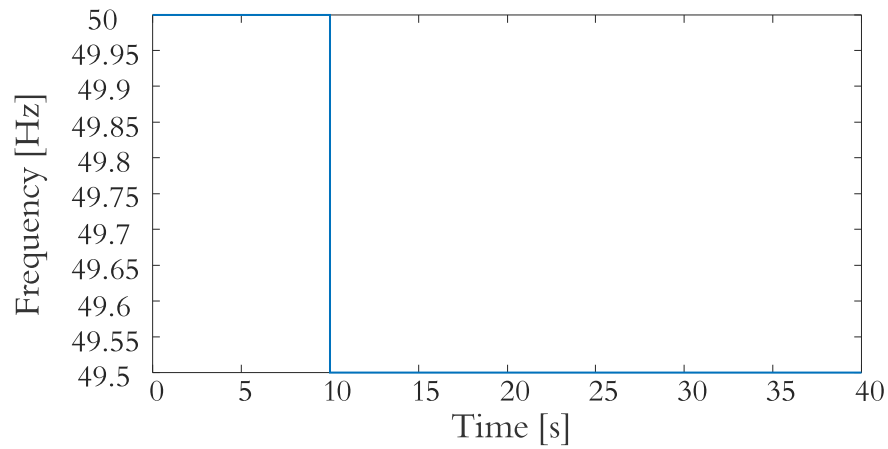
Figure 4-2: Step response of modelled primary frequency control.
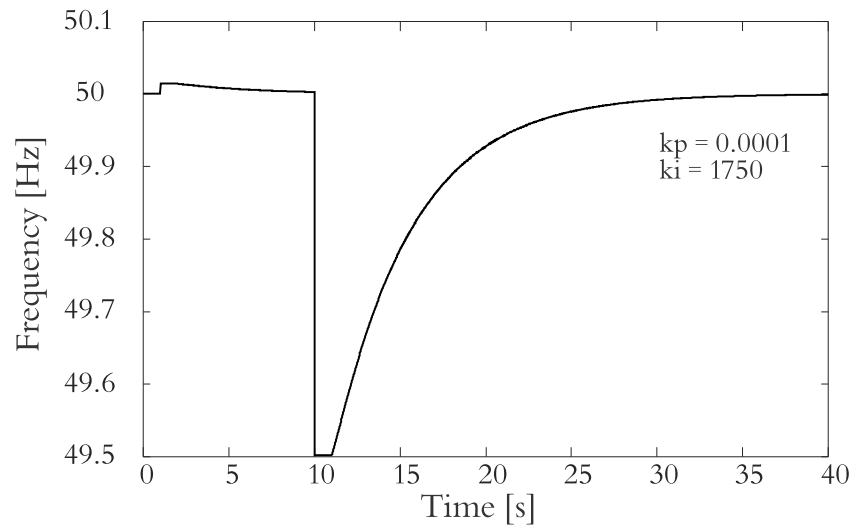
Figure 4-3: Transient response of the secondary control model for frequency restoration.

4.2 Voltage primary and secondary control model

Similar procedure has been applied when designing the voltage secondary controller model. Fig 4-4 shows the block diagram obtained in this case. Similarly, we get the

closed-loop voltage dynamic model.
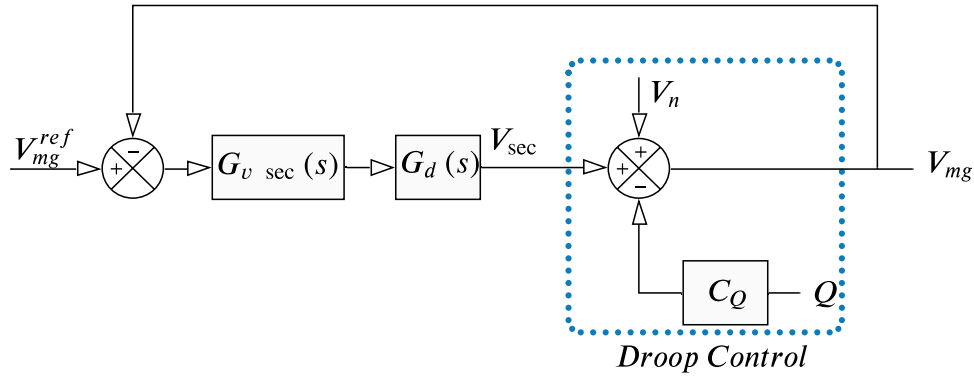
Figure 4-4: Block diagram of the simplified voltage secondary control model[7].

$$V_{mg} = \frac{G_{v\ sec}(s)\,G_d(s)}{1 + G_{v\ sec}(s)\,G_d(s)} V_{mg}^{ref} - \frac{C_Q}{1 + G_{v\ sec}(s)\,G_d(s)} Q \qquad (4.2)$$

Fig 4-5 shows the step response for a change in Q (reactive power total load) from 0 to 50kVAr at 10s of just the primary voltage droop control in Fig 4-4 and Fig 4-6 depicts the step response of the modelled primary and secondary control in Fig 4-4 for the same load condition. Primary control response in Fig 4-5 limits the change in voltage, but it does not bring back the system voltage back to nominal value (326.6 V), but primary and secondary control combine brings back the system voltage back to nominal value, shown in Fig 4-6. This model helps to adjust properly the control parameters of the secondary voltage control and to study the limitations of the communication channel delay.

4.3 Improvement in secondary control response by Smith Predictor

To improve the secondary control transient response shown in Fig 4-1 and 4-4, where it takes more than 25s to settle to nominal value due to a step change in P and Q respectively, another improved secondary control model is suggested with smith
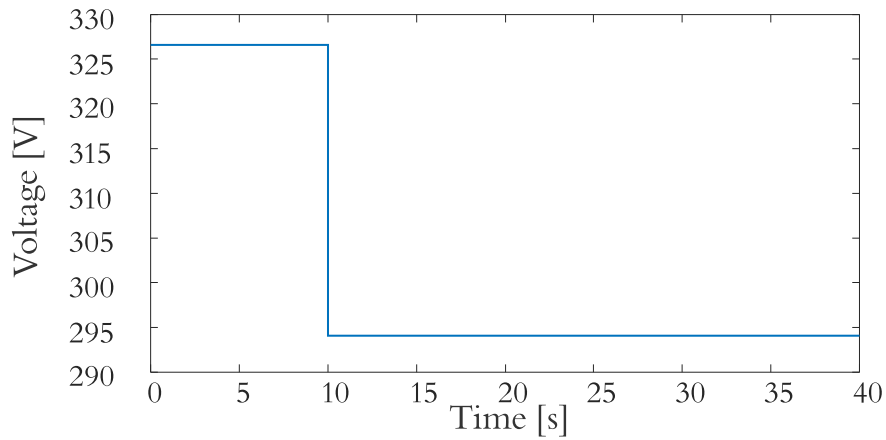
Figure 4-5: Step response of modelled primary voltage control.
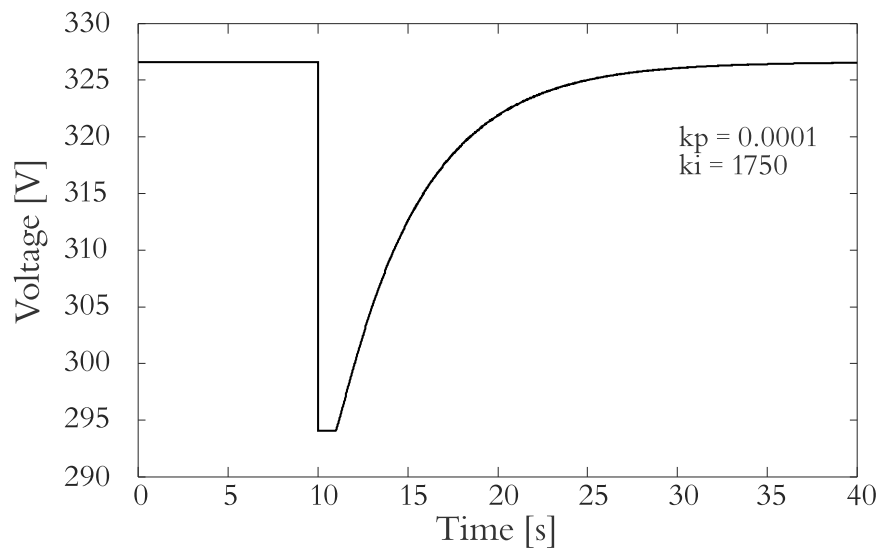
Figure 4-6: Transient response of the secondary control model for voltage restoration.

predictor. The theory and working principal behind smith predictor is covered in Chapter 2.6.

Fig 4-7 and 4-9 shows the block diagram of the improved secondary control with smith predictor. Fig 4-8 and 4-10 shown the comparison results between the two control methods. It is clear from both the response figures that smith predictor can improve the transient behaviour of the secondary control drastically. As it can be seen in the green graph in both the comparison plots, the system reaches nominal

Figure 4-7: Block diagram of the simplified smith predictor frequency secondary control model.

Figure 4-8: Comparison of transient response of the frequency secondary control for frequency restoration.

value in about 3s, which is way faster than the first method without smith 25s. This is because smith predictor allowed to improve the PI controller gain values (Kp = 0.0005) and (Ki = 5000) respectively without hampering the system stability. On the other hand, the red plots in the comparison graphs shows that the previous systems without smith becomes unstable if is subjected to (Kp = 0.0005) and (Ki = 5000). In summary, Fig 4-8 and 4-10 shows both improvement in transient response compared to 4-1 and 4-4 by smith predictor and comparison of stability at higher gain vales for both the control methods.

Figure 4-9: Block diagram of the simplified smith predictor voltage secondary control model.
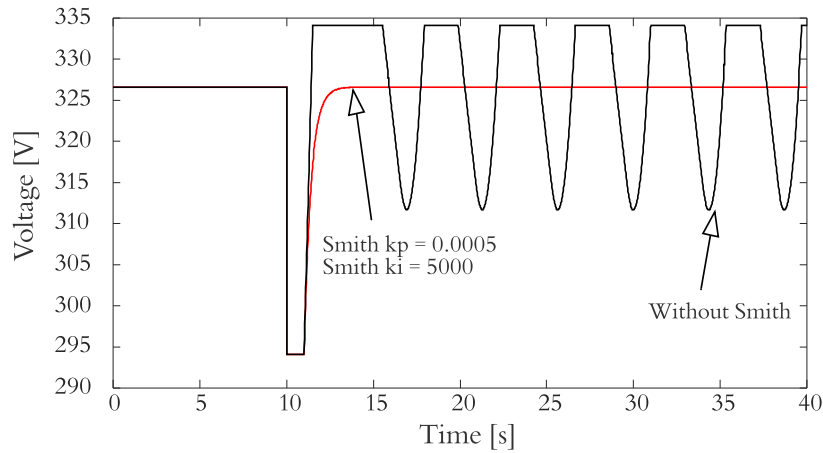
Figure 4-10: Comparison of transient response of the voltage secondary control for voltage restoration.

4.4 Microgrid primary and secondary control island mode

Based on the theory of Smith Predictor covered in chapter 2 and implemented in simplified models in Fig 4-1, 4-4, the DHEMS in Fig 2-9 is modified with the block diagram shown in Fig 4-11
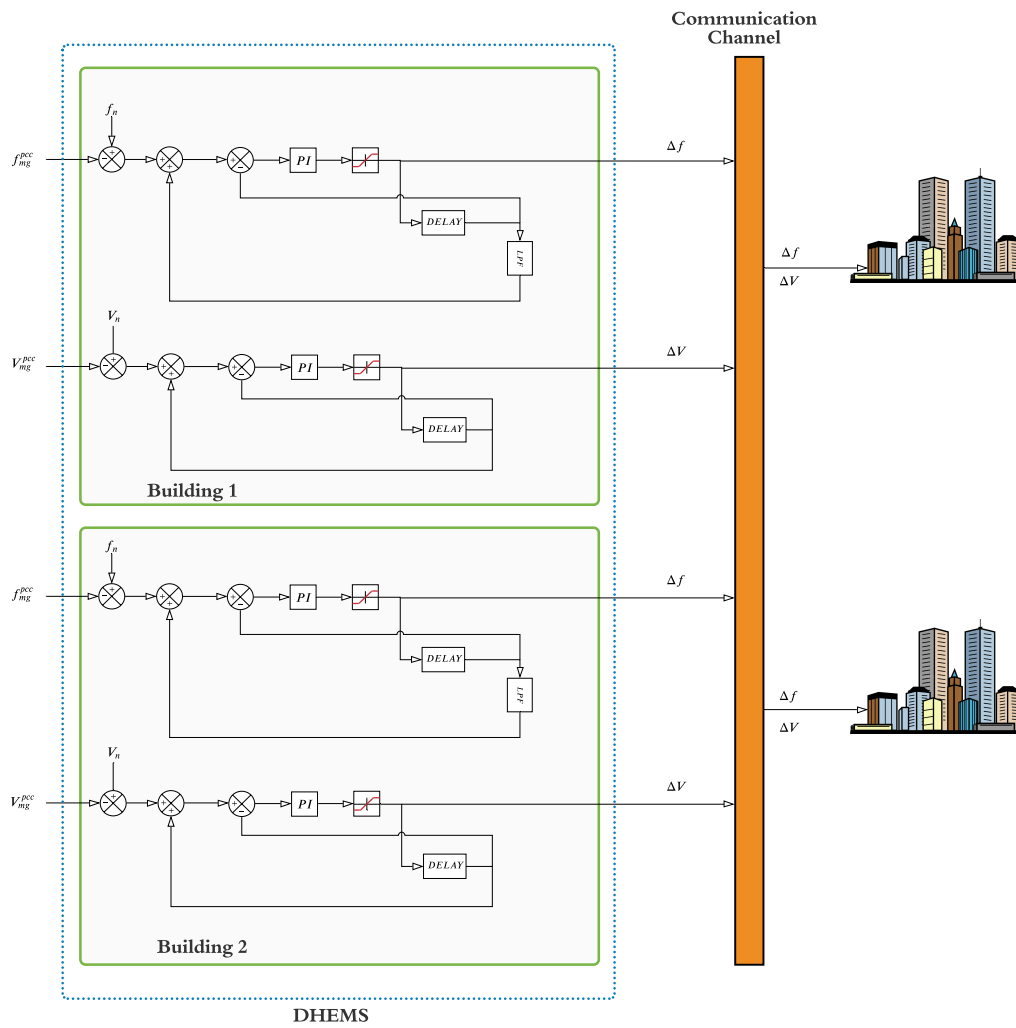
Figure 4-11: Improved secondary controller in DHEMS.

4.4.1 Simulation results of island

Fig 4-12,4-13 shows the active and reactive power of building 1,2,3 and PCC. The first 3s there is no load operation, then at 3s resistive load is turned on and then switched off again at 10s. From 10s to 15s, there is no load. Finally, at 15s inductive load tuned on. Due to this load profile of active and reactive power consumption voltage and frequency at building and PCC of the MG also deviates from the nominal value. At no load condition, the system voltage and frequency remains at 326.6V and 50Hz. At 3s, the resistive load is turned on. The PCC node and building 3 node voltage drops instantly, but the building 1 and 2 nodes main the voltage to nominal as we did not consider loads inside the building 1 and 2. Information from the PCC takes one second to reach the building 1 and 2 (prosumers), they start generating power to supply the load demand. Hence from 4s onwards, prosumer node voltages rises in an attempt to keep the PCC node voltage at nominal. At 10s, as there is again a change in load, PCC voltage deviates from nominal. The prosumer (Building 1 and 2) takes 1s to react again and everything get to nominal. At 15s, when there is a reactive power demand, also in this case similar situation occurs only this time the prosumer buildings supply inductive power to keep the PCC at nominal voltage. Similarly, the transients in Fig 4-15 can be explained using the same argument mentioned above.

4.5 Microgrid primary and secondary control grid connected mode

This section presents the simulation results of the microgrid in grid connected mode. Simulink model of the Synchronization of the MG PCC with the main grid is shown in Fig B-6. Fig 4-16 shows the block diagram of the microgrid with the main grid. Voltage and phase from the PCC and main grid are compared and passed though PI controller for voltage and just an integral control for phase respectively. Unramp block is used for phase as shown in the block diagram in Fig 4-16. The V_{sync} and f_{sync} signals are then added to the secondary control reference. When the PCC voltage
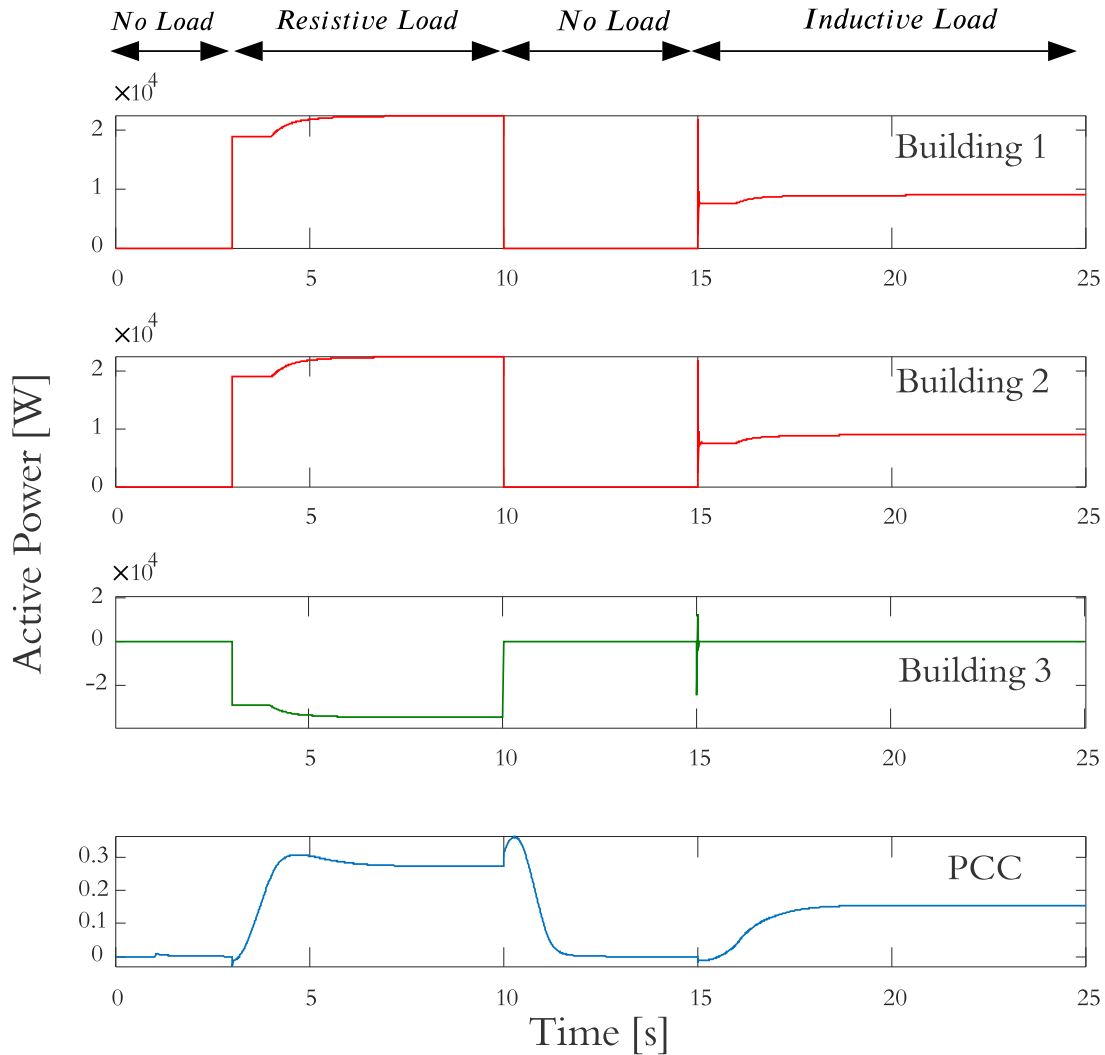
Figure 4-12: Active power of buildings and PCC.

and phase is matching the grid voltage and phase the circuit breaker in closed. In the remaining simulations results, breaker is always closed at 13s.

Active and reactive power profiles are shown in Fig 4-17 and 4-18.Inductive load was turned on between 3s to 10s. Grid is connected to the main grid at 13s and a resistive load was connected from 15s to 25s. Fig 4-19 and 4-20 captures the performance of the system in grid connected mode. Till 13s the simulation results are similar to previous section results as the MG operates in island mode, when the grid is connected at 13s and a resistive load demand is applied at 15s, the system becomes unstable for about 3s and then the secondary control stabilizes the system to nominal value.
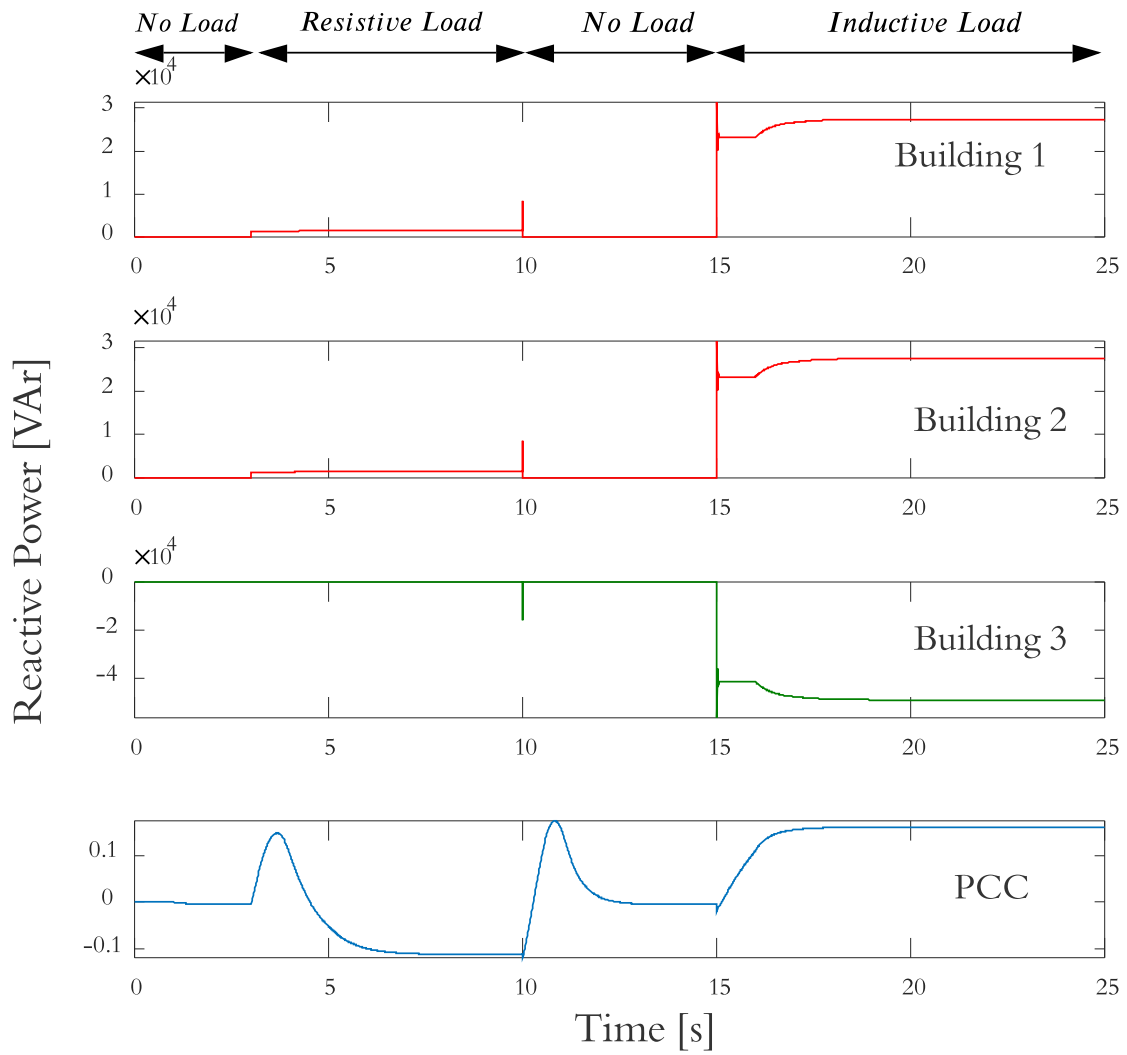
Figure 4-13: Reactive power of buildings and PCC.
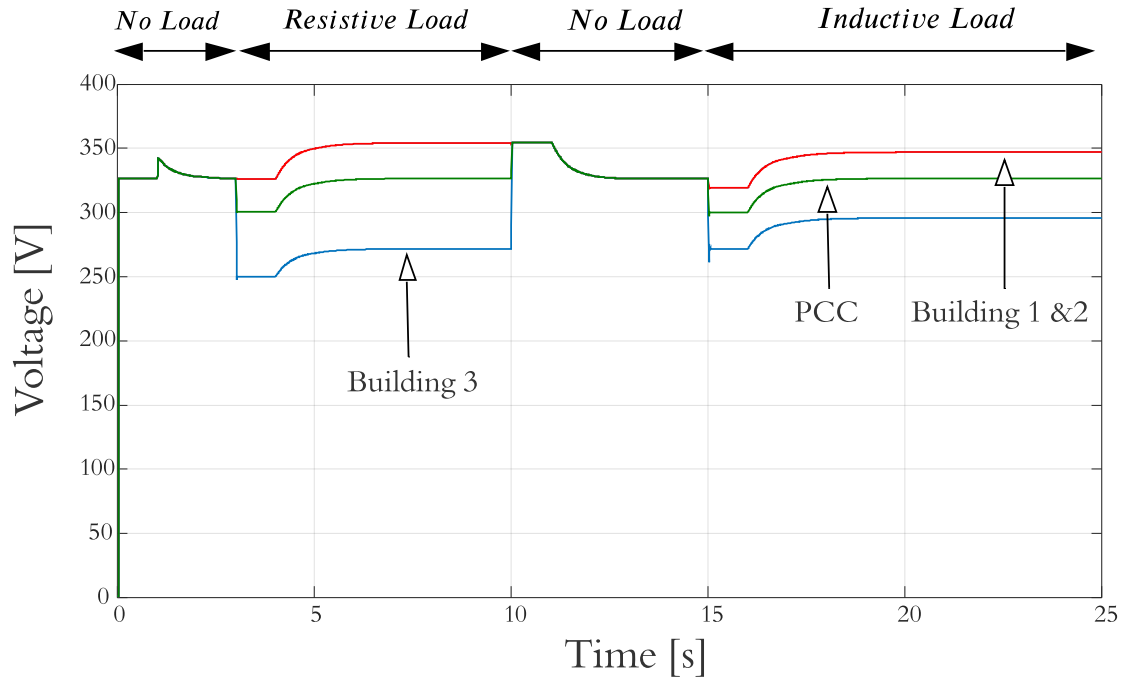
Figure 4-14: Voltage of buildings and PCC.
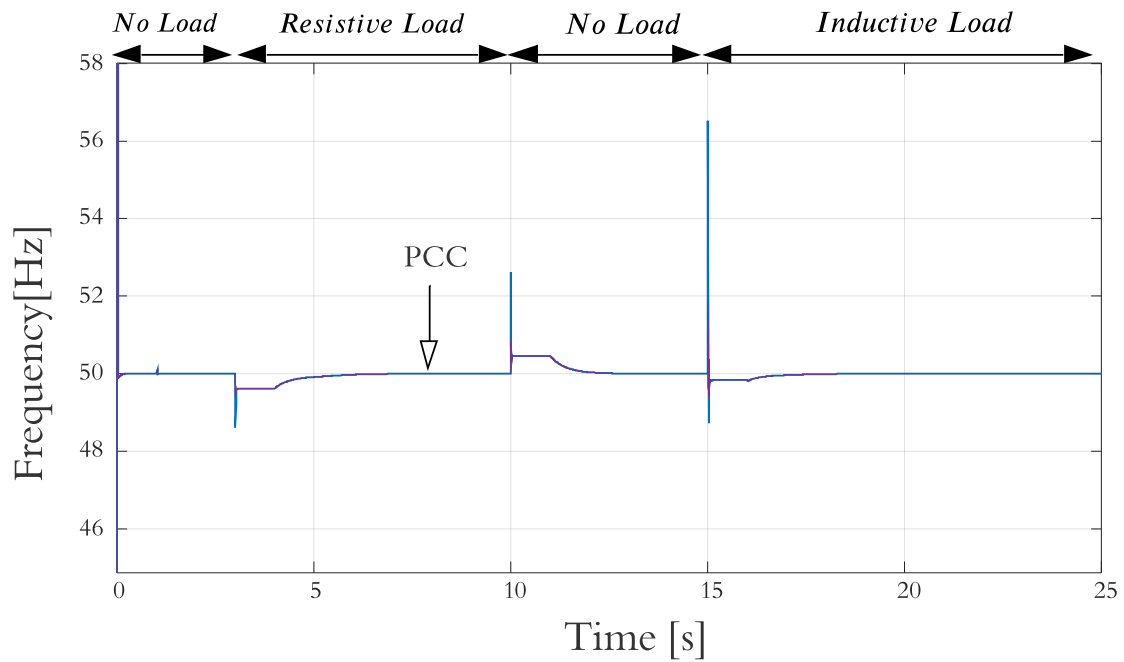
Figure 4-15: Frequency of buildings and PCC.
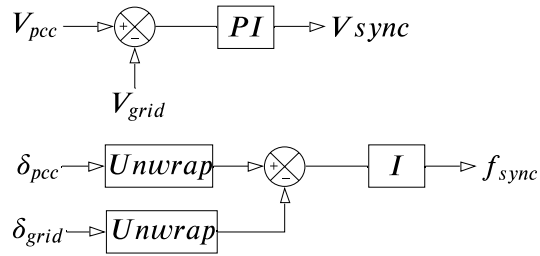
Figure 4-16: Block diagram of synchronization of the microgrid with main grid.
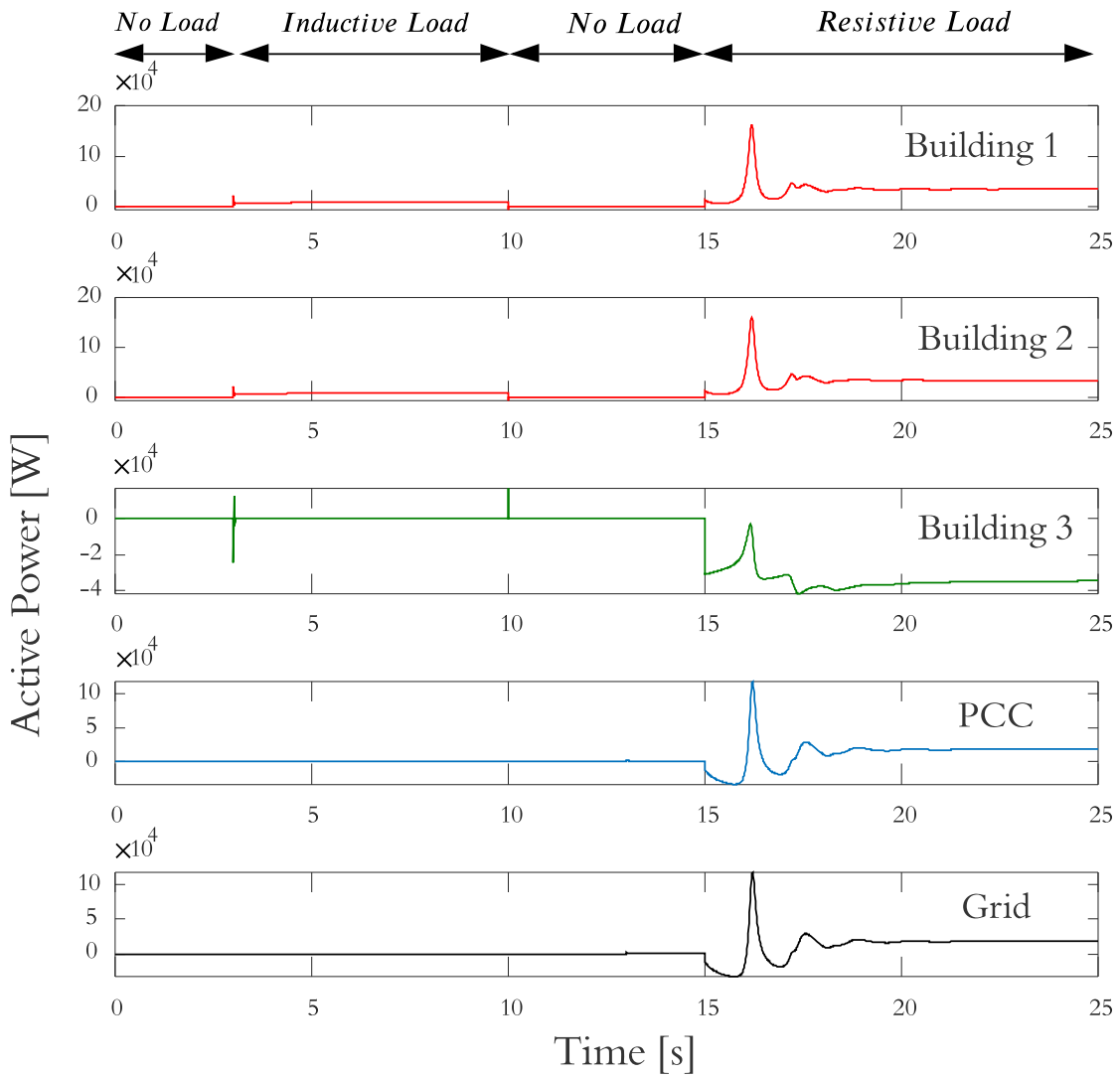
Figure 4-17: Active power of buildings,PCC and grid.
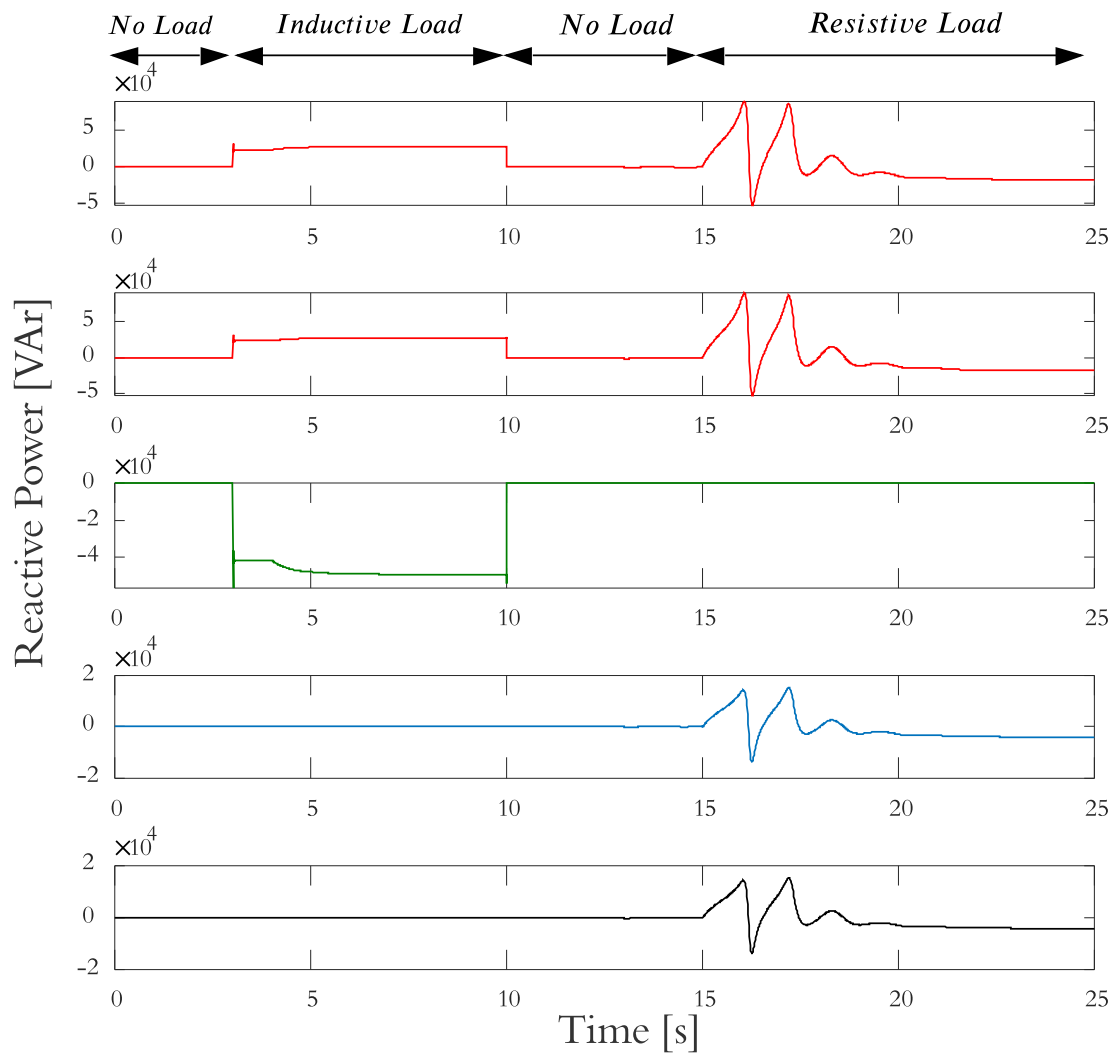
Figure 4-18: Reactive power of buildings,PCC and grid.
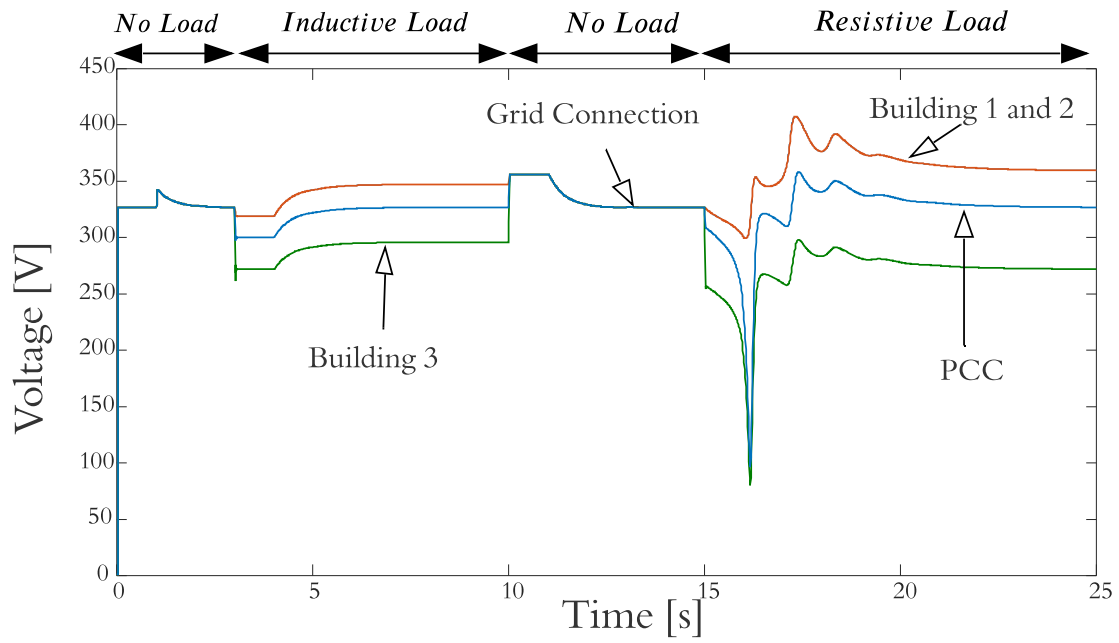
Figure 4-19: Voltage of buildings and PCC.
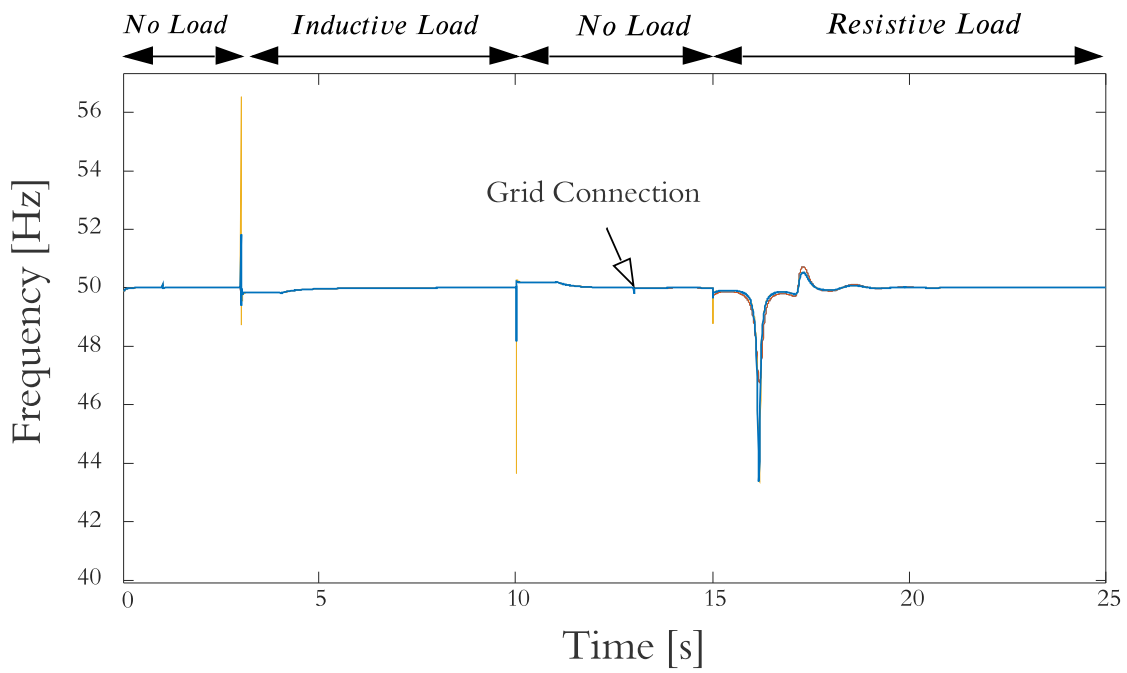
Figure 4-20: Frequency of MG.

61

Chapter 5

Simulation and Design of Microgrid Communication Channel

This chapter explains the modelling of the communication delay using Poisson distribution. It also compares Smith Predictor guessing the communication delay versus fixed delay of 1s in the DHEMS. Results of communication outages of building are also checked.

5.1 Modelling of variable delay communication channel using poison distribution

A typical communication channel will not behave ideally like we have assumed through the discussion. It will rather behave like shown in Fig 5-1, where there is a fixed delay, i.e, in our case 1s, but most of the time there will variation of the delay time as shown in that figure. Some information may take too long to be delivered as well or may be lost. The best way to represent the typical communication channel behaviour shown in 5-1 is using Poisson distribution. In the upcoming sections simulation results of variable delay under different condition is presented.
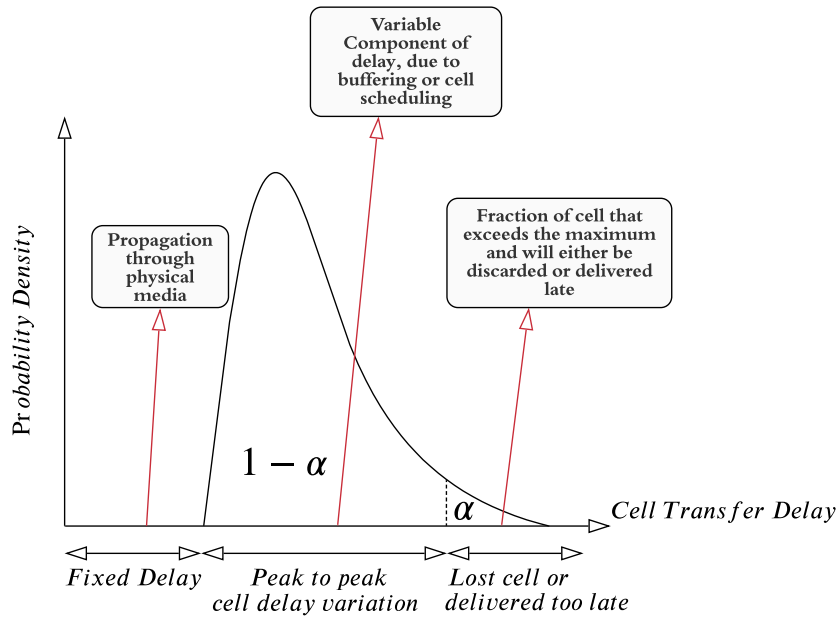
Figure 5-1: Characteristics of a typical communication channel.

5.2 Simulation of secondary control with variable delay

Fig 5-2 shows the histogram of variable delay used in the simulation results below. It can be seen that the Fig 5-2 tries to mimic Fig 5-1 so that a close approximation to Poisson distribution is achieved. The histogram in Fig 5-2 represents variable delay of 1.3s for about 38% of the simulation (which can be considered as the peak of the Poisson distribution) and it also has 2.3s and on wards for about 0.5% of the simulation which can be represented as information lost or delivered too late.

Fig 5-3 shows the simple method to make the Poisson distribution delay, which is used to test the system in the upcoming sections and delay values are presented by the Poisson distribution graph shown in Fig 5-2. Similar load profile to the one used in chapter 4.4.1 was used also used in this simulation as well. Fig 5-4 and 5-5 shows the active and reactive profile of buildings and PCC.

Fig 5-6 and 5-7 shows the control response of the system in voltage magnitude and frequency when variable delay generated by Fig 5-3 is injected in the system instead
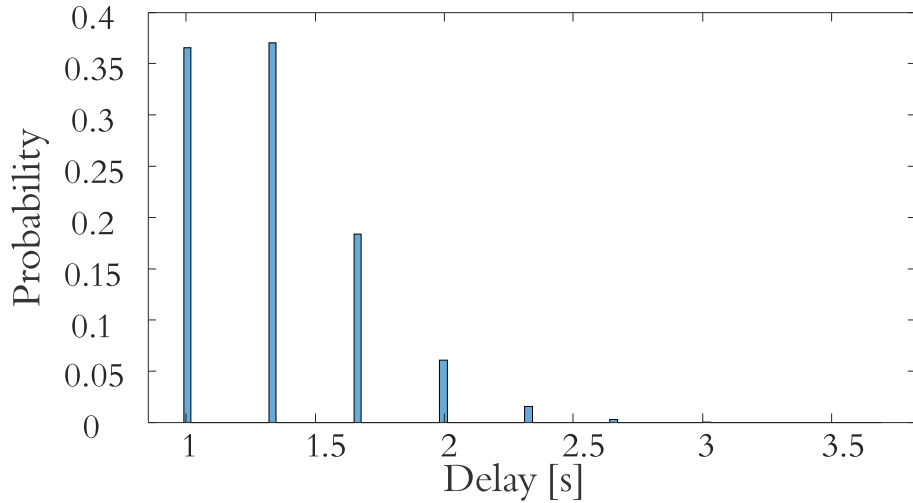
Figure 5-2: Histogram of variable delay used in simulation based on Poisson distribution.
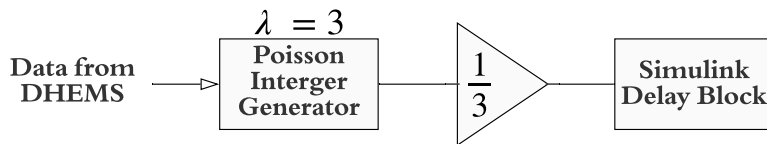
Figure 5-3: Schematic of simulink model to create variable delay.

of a constant delay of 1s.

As seen in Fig 5-6 and 5-7 the system is stable even with variable delay. It takes longer time to reach the nominal value than the system of constant delay of 1s as in Fig 4-14 and 4-15. The conclusion from the comparison of these plots is the systems proposed is stable even with variable delay (emulating real world situation).

5.3   Simulation results for delay prediction inside DHEMS

Similar load profile is used again to check the voltage and frequency response had case delays in DHEMS were able to guess the delay variations. Fig 5-8 and 5-9 shows voltage magnitude and frequency response of the system. It can be seen from the figures that if the delays in DHEMS are able to guess the delay variation, the response is improved drastically.
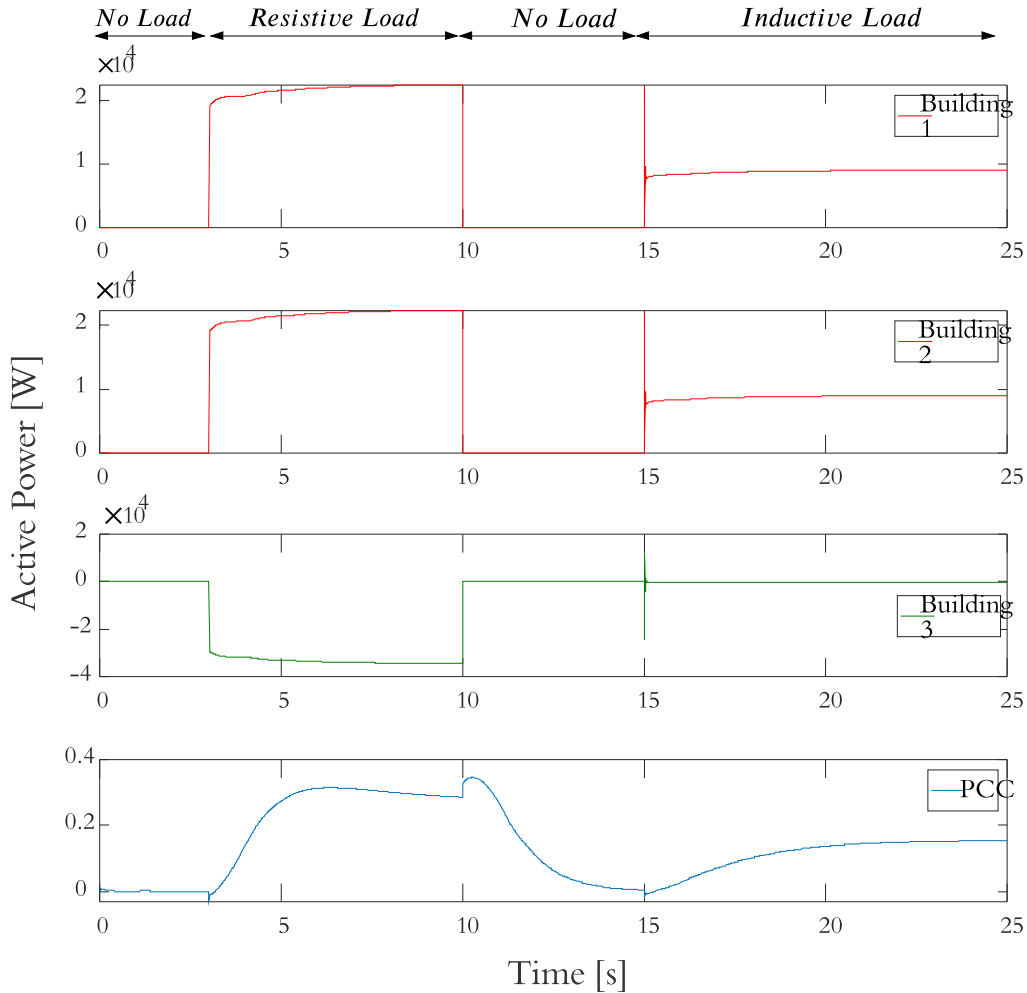
Figure 5-4: Active power profile of buildings and PCC with variable delay.

5.4 Simulation and analysis of communication channel outage in buildings

This section covers the simulation results and discussion for the outage in one of the buildings. The load profile shown in Fig 5-10 and 5-11 is the same as used for variable delay simulation. The outage takes place at 8s in building 2. This is seen in Fig 5-12 at 8s, when the voltage in building 2 (red plot) drops to nominal value. Active power graph shown in Fig 5-10 shows that building one has to generate excess power should was supposed to be generated by building 2 which lost connection. Another transient can be seen in all the figures of this section at 13s, this is due to the connection of
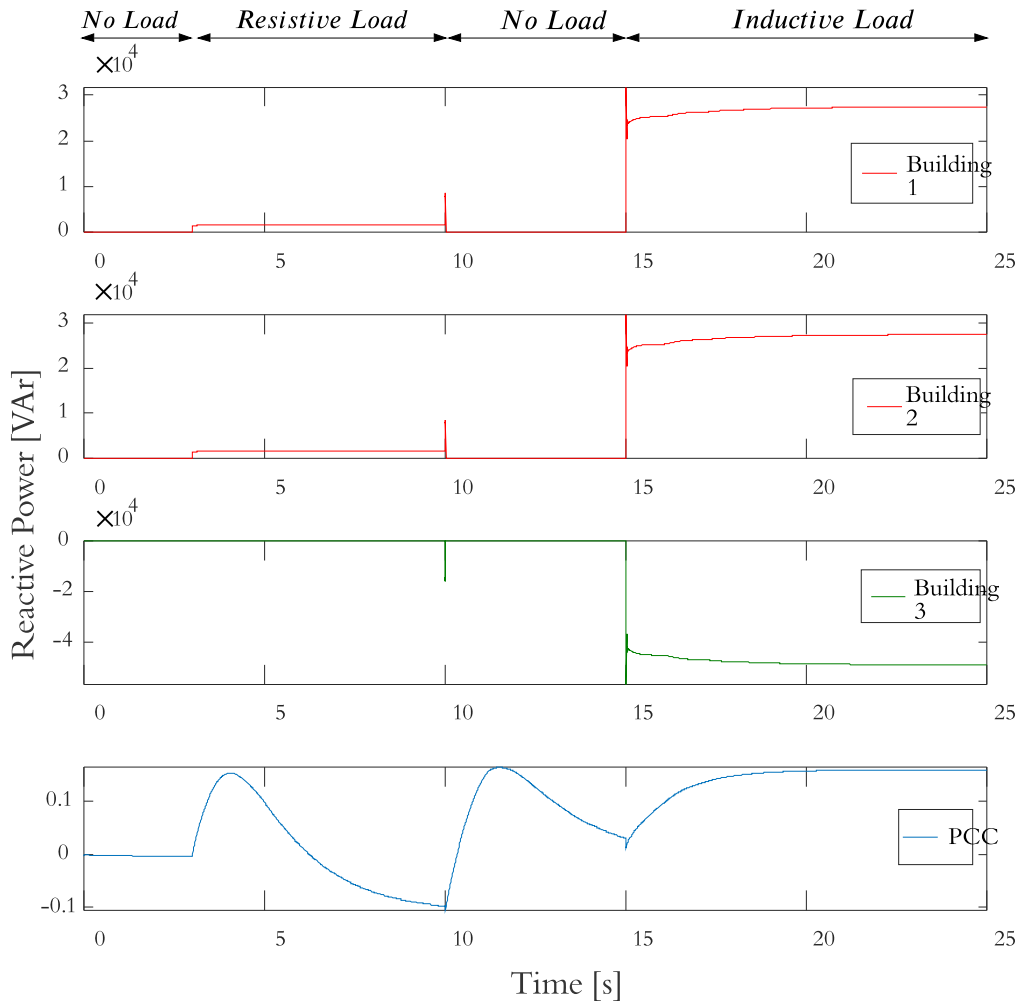
Figure 5-5: Reactive power profile of buildings and PCC with variable delay.

the main grid in the microgrid.
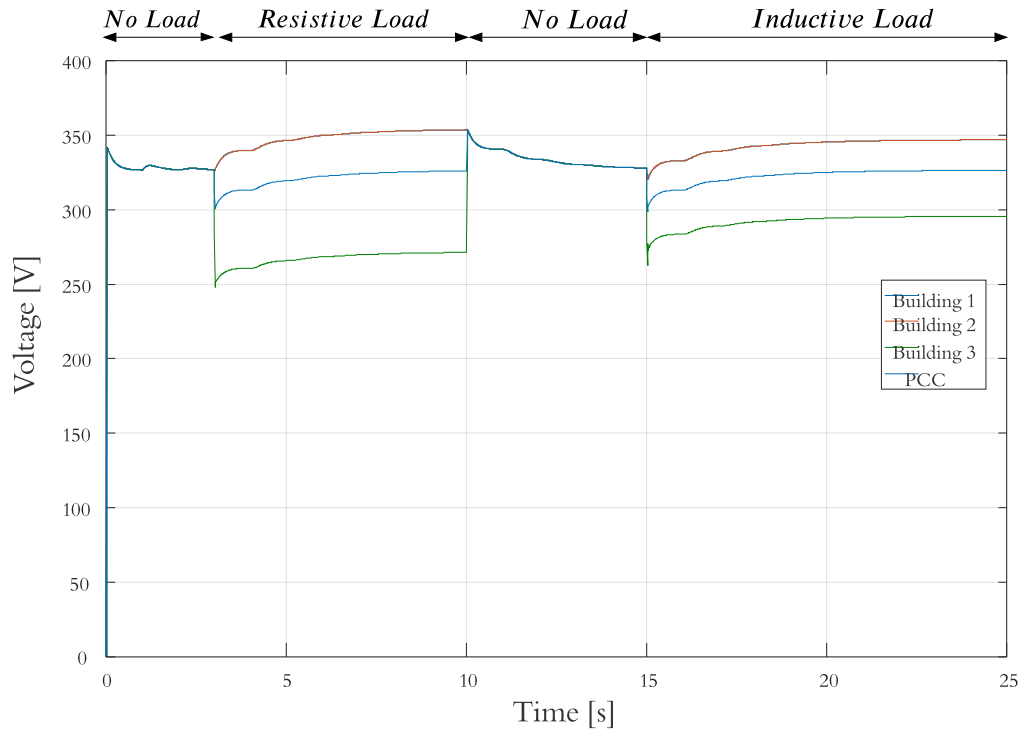
Figure 5-6: Voltage response of the system with variable delay.
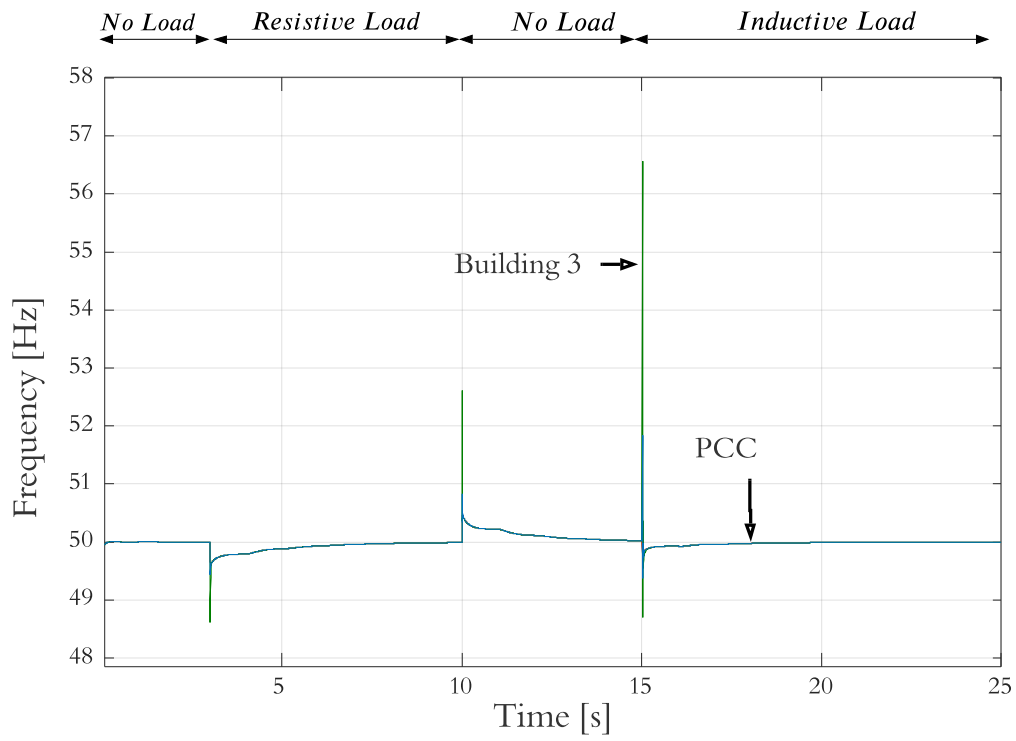
Figure 5-7: Frequency response of the system with variable delay.

68
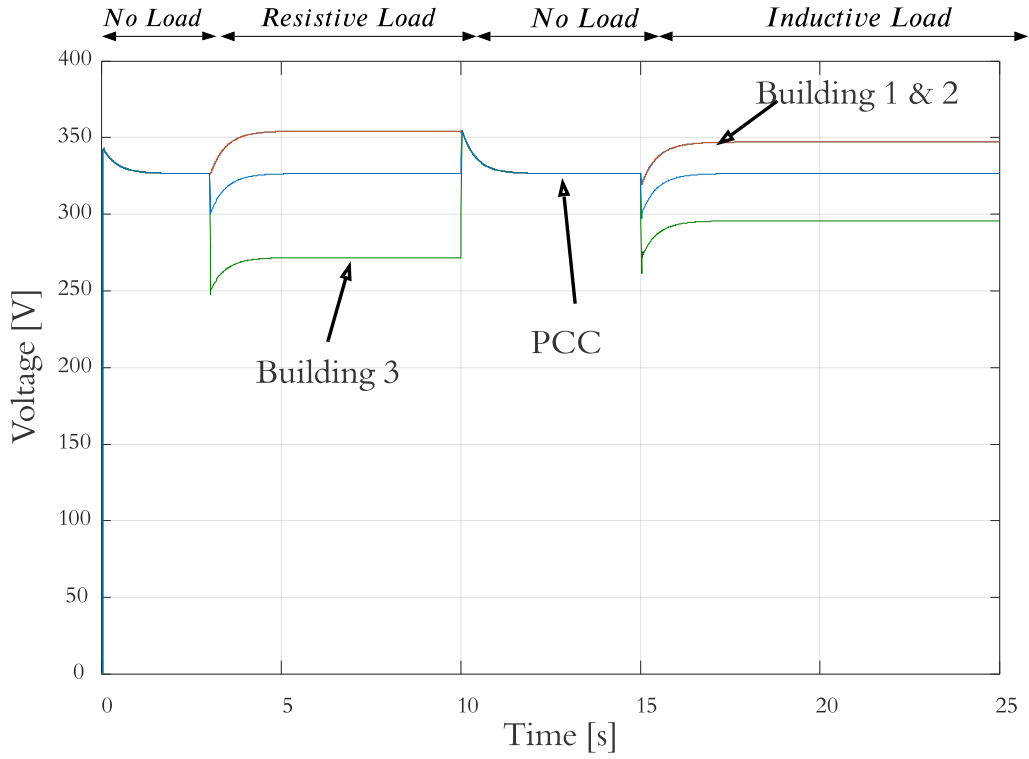
Figure 5-8: Voltage response of the system with variable delay in DHEMS.
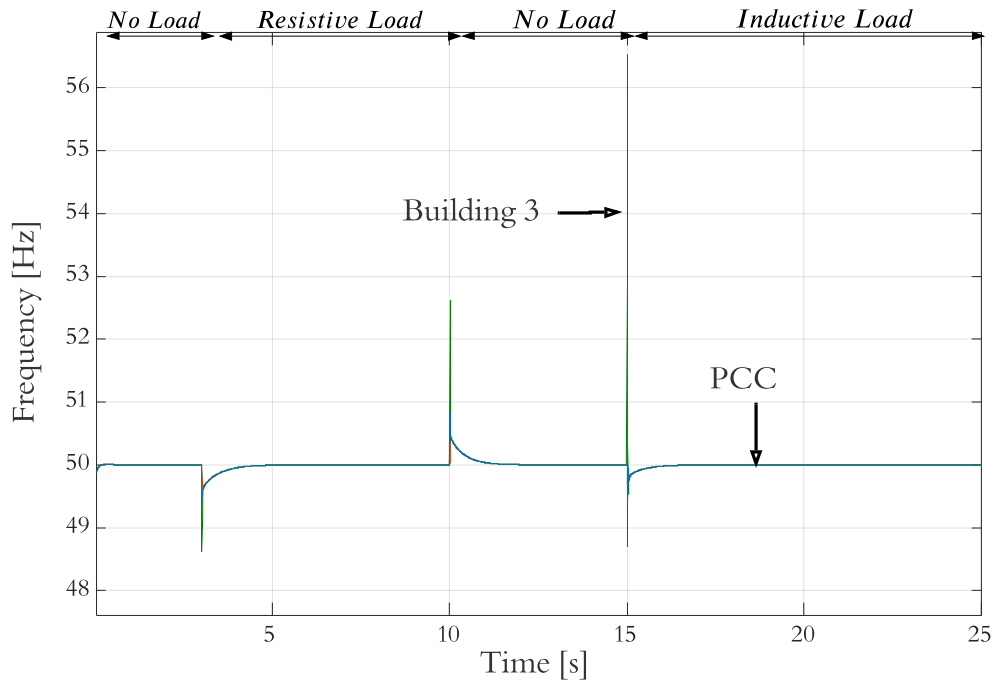
Figure 5-9: Frequency response of the system with variable delay in DHEMS
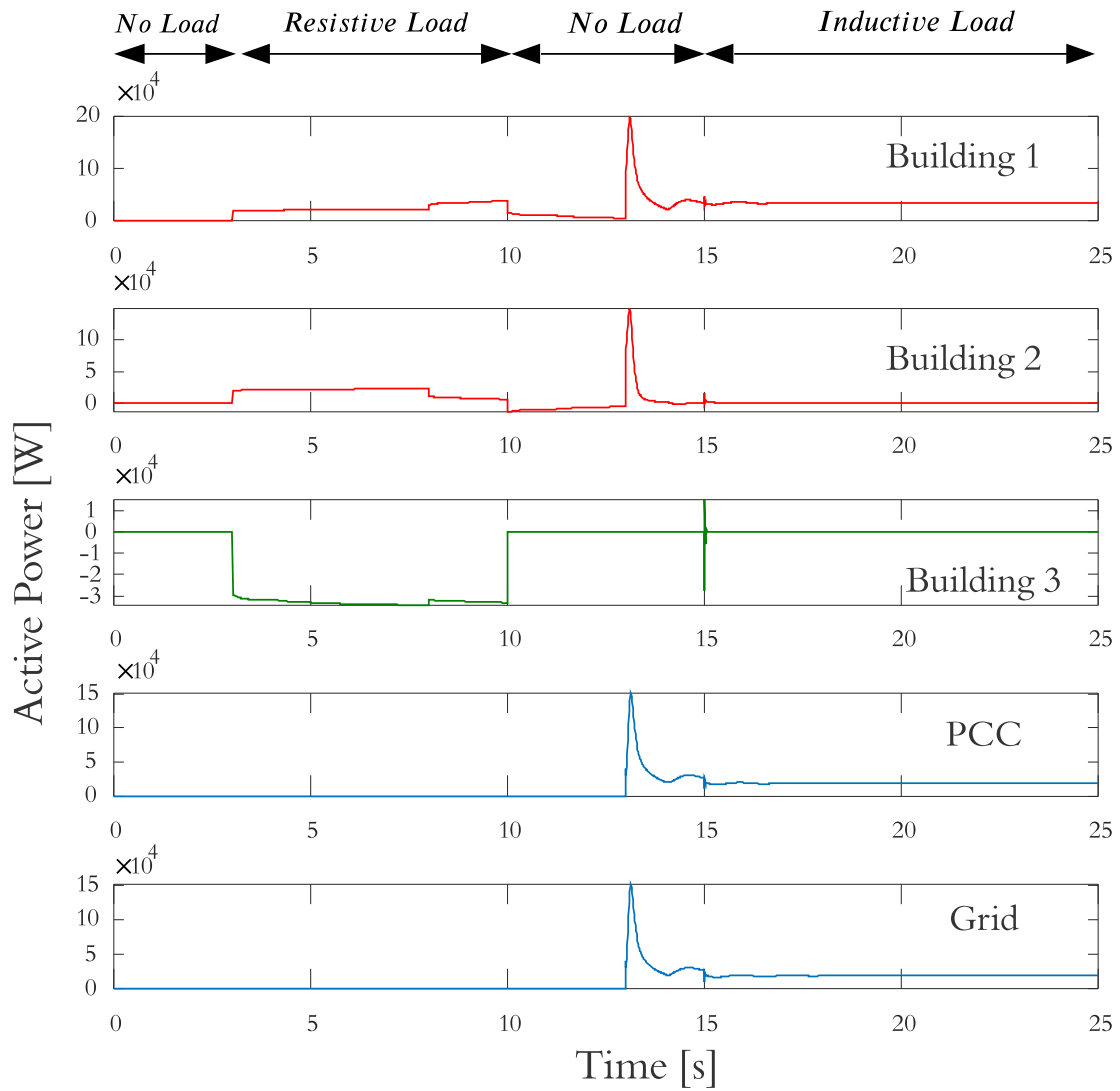
Figure 5-10: Active power profile for communication outage simulation.
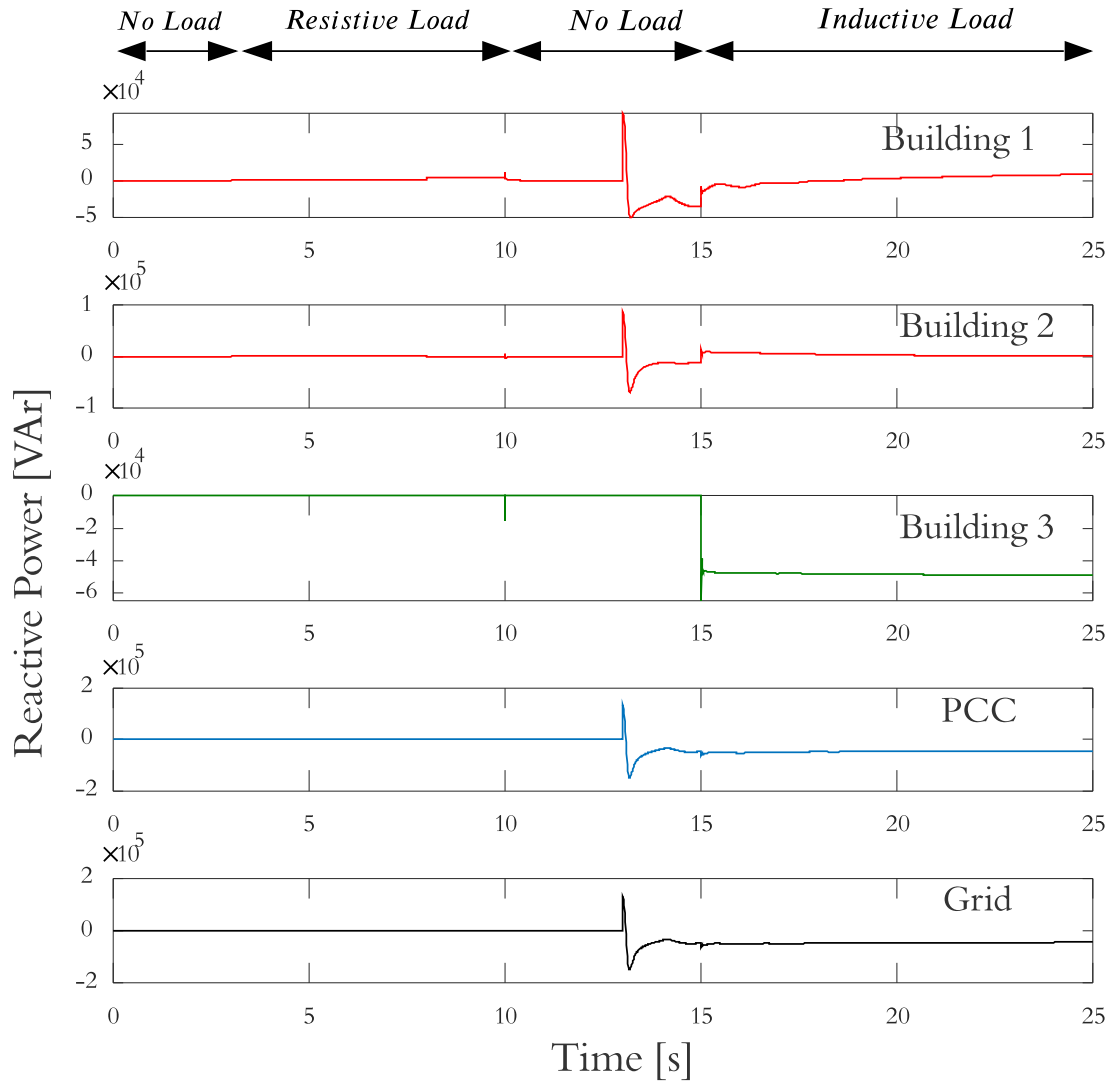
Figure 5-11: Reactive power profile for communication outage simulation.
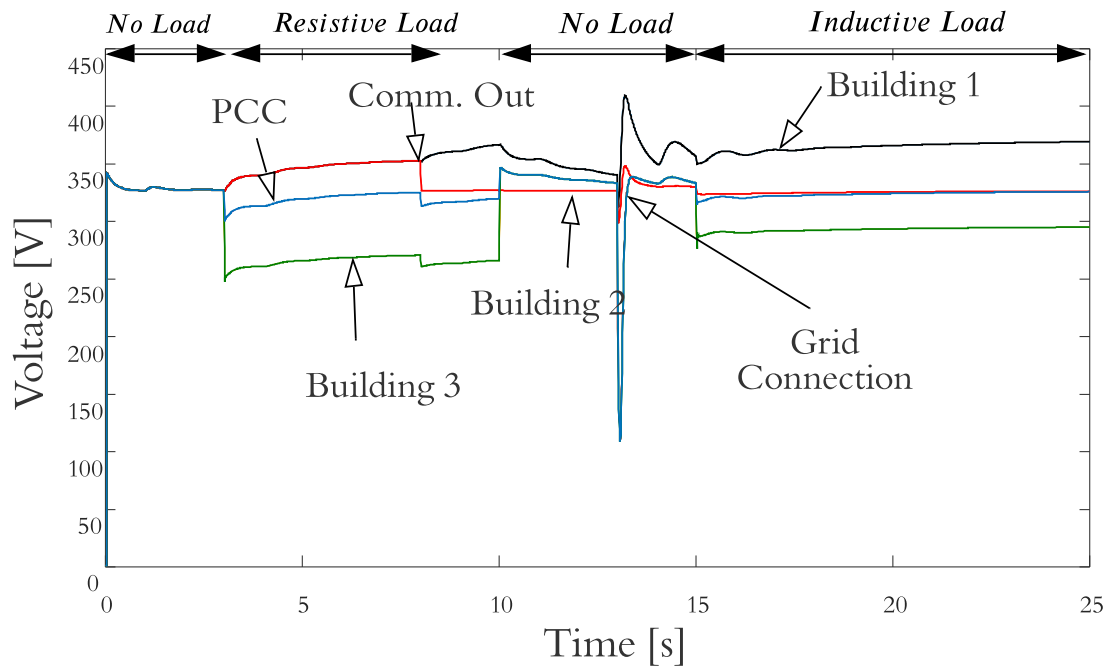
Figure 5-12: Voltage response due to communication outage.
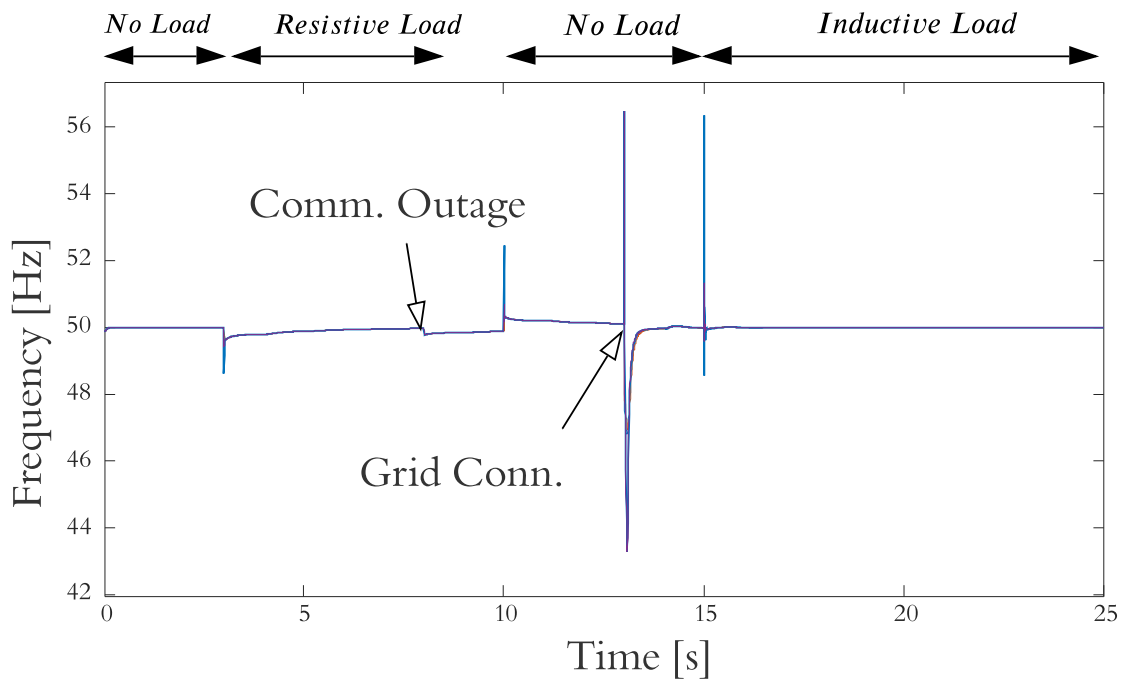
Figure 5-13: Frequency response due to communication outage simulation.

Chapter 6

Microgrid Tertiary Control Modelling and Control Design

This chapter explains the microgrid tertiary control modelling and simulation results of both the modelled tertiary system and the original system explained in chapter 3.

6.1   Simplified model of tertiary control for turning the PI gains

A simplified model of tertiary control shown in Fig 2-16 has been made to understand the range of the tertiary PI controller gains of the overall system as it takes shorter time to simulate. Fig 6-1 shows the overall hierarchical multi-building MG control. The gains for secondary control is the same as used in Fig 4-7 and 4-9.

The simplified grid model shown in Fig 6-1 has been made by using the two active and reactive power equations 6.1 and 6.2 respectively.

$$P_{OUT} = \frac{-V_{mg}V_{grid}}{X} \sin\left(\delta_{grid} - \delta_{mg}\right) \tag{6.1}$$

$$Q_{OUT} = \frac{-\left(V_{grid}\right)^2}{X} + \frac{V_{mg}V_{grid}}{X} \cos\left(\delta_{grid} - \delta_{mg}\right) \tag{6.2}$$
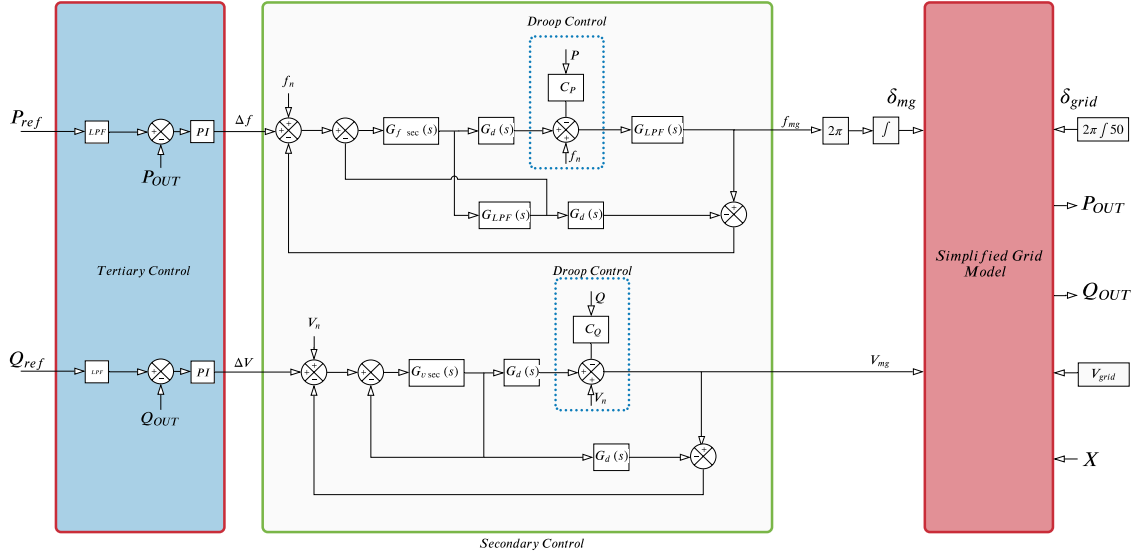
Figure 6-1: Simplified model of hierarchical multi-building MG control.

where, V_{mg} is the microgrid voltage at PCC, V_{grid} is the grid voltage, δ_{mg} is the microgrid phase angle at PCC, δ_{grid} is the grid phase angle and X is the grid impedance. δ_{mg} is calculated by the the frequency output from the secondary control in Fig 4-7 and integrating it and then multiplying it by 2π as shown in equation 6.3. Similarly δ_{grid} is calculated by integrating $f_n(50Hz)$ and multipling it with 2π as shown in equation 6.4.

$$\delta_{mg} = 2\pi \int f_{mg} \tag{6.3}$$

$$\delta_{grid} = 2\pi \int f_n = 2\pi \int 50 \tag{6.4}$$

6.1.1 Simulation results of the simplified model tertiary system

Fig 6-2 and 6-3 shows the step response of the tertiary control of the propose simplified system of the hierarchical MG control. P_{ref} and Q_{ref} should come from EMS based on the optimum performance of the MG. Reactive Power tracks the reference between than Active power as there are relatively less transients. Active Power takes more

74
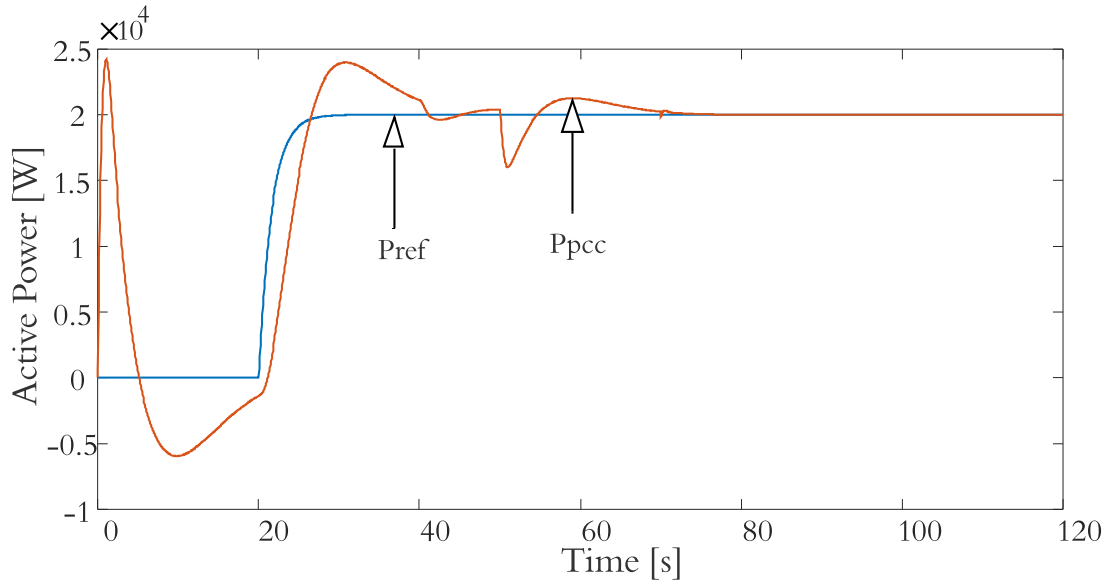
Figure 6-2: Active Power response of the simplified tertiary controller.
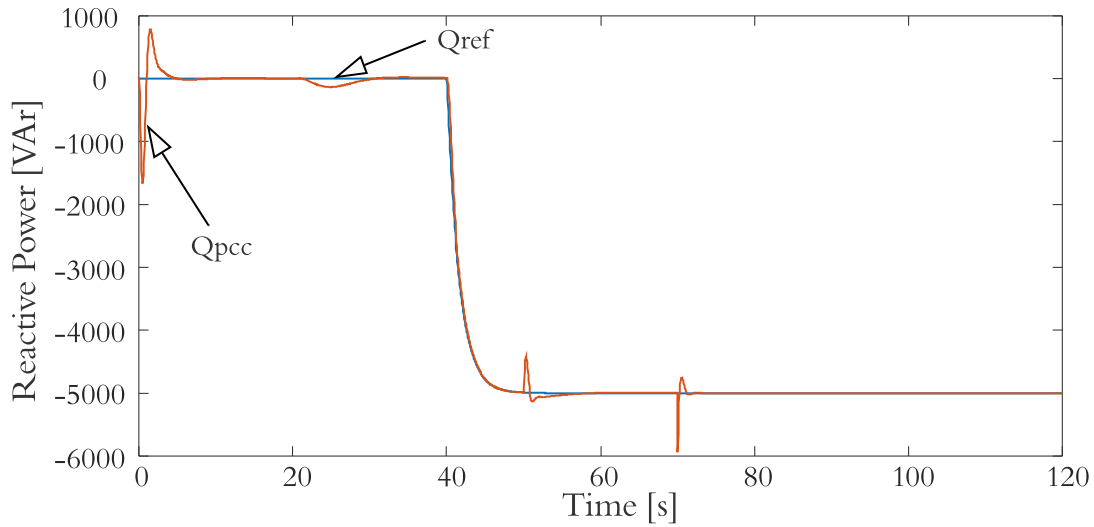
Figure 6-3: Reactive Power response of the simplified tertiary controller.

time to be stabilized. In Fig 6-2 a step input reference of active power demand 0kW to 20kW happens at 20s, since the system is slow it takes 55s to stabilize and meet the requirement. The spike at around 40s is due to the step change in reactive power reference. Whereas, in Fig 6-3 a step input of reactive power reference from 0 kVAr to -5 KVAr is met. Few transients we observe here is due to the poor performance of

the active power tracking.

6.2 Tertiary control performance analysis

Now that we have found the range of the gains values for G_{pP},G_{iP},G_{pQ} and G_{iQ} from the simulation of 6-1, we can put these values in the original hierarchical MG shown in Fig 6-4. Active and Reactive Power is measured from the PCC and it is then compared with reference Active and Reactive Power send by the EMS based on its calculation to have the most economically feasible operating MG.
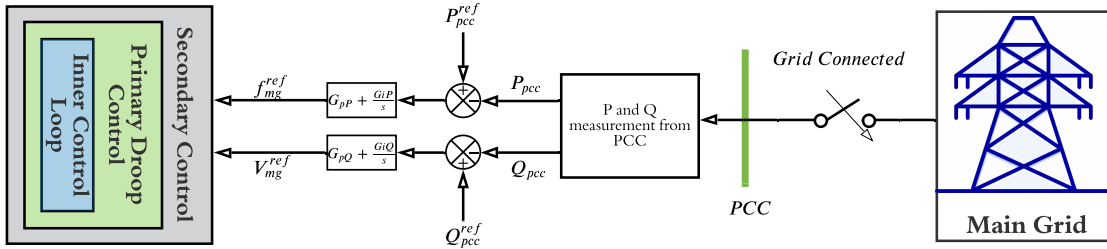
Figure 6-4: Structure of tertiary control in microgrids[5].

6.2.1 Simulation results of the proposed tertiary control systems

Fig 6-5 and 6-6 shows the control reponse of tertiary control for the full system shown in Fig 2-16. The control is very slow and step change in active power take more than 20s to stabilize and this also causes reactive power to destabilize. Step change in reactive control is more stable and impacts very less in active power control. Possible improvements are suggested in chapter .
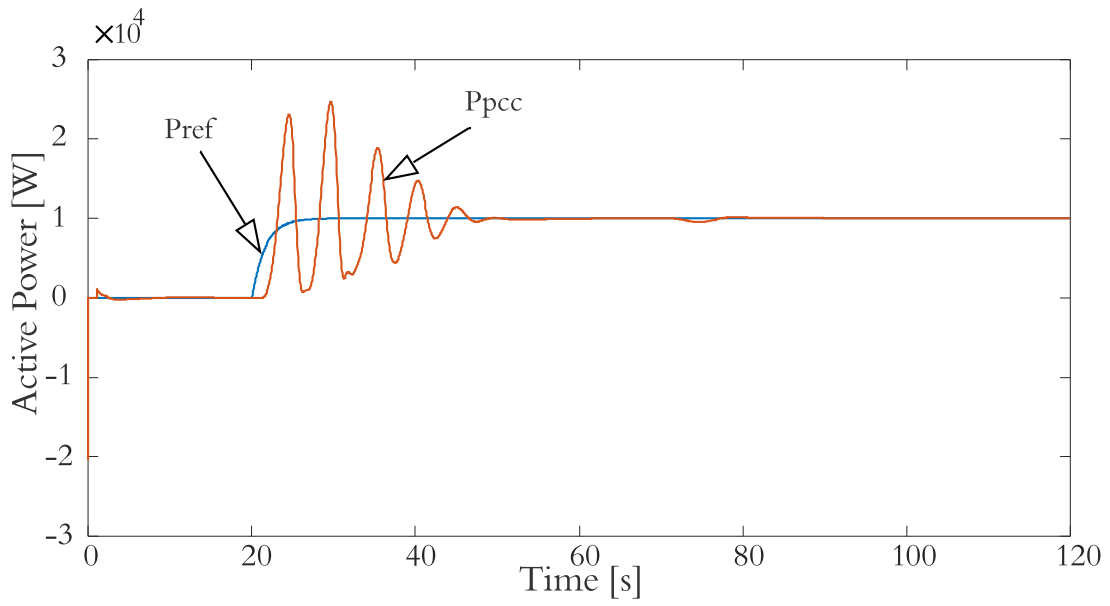
Figure 6-5: Active Power response of the tertiary control.
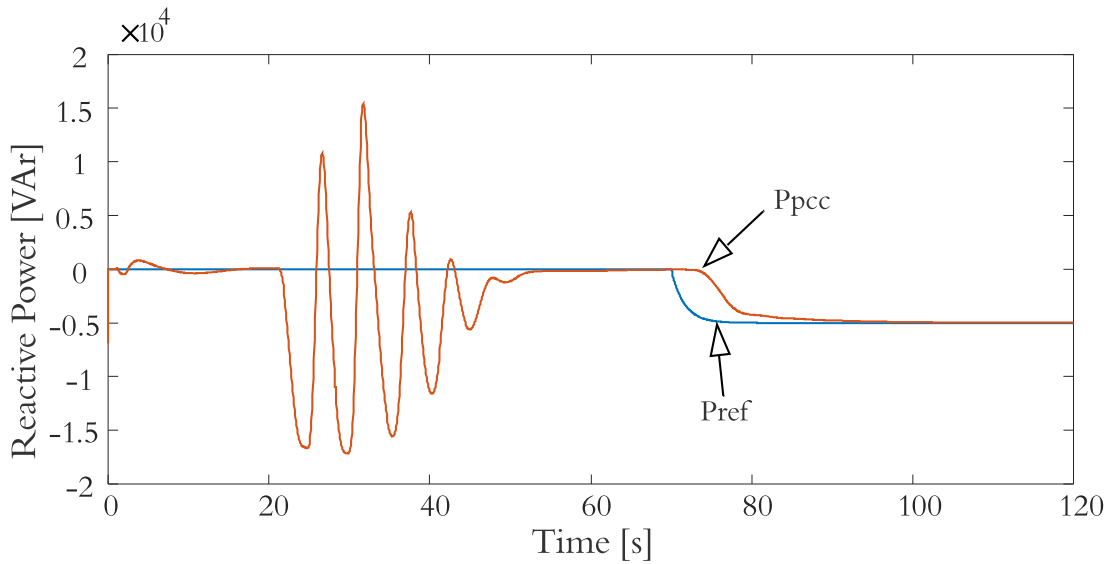
Figure 6-6: Reactive Power response of the tertiary control.

Chapter 7

Conclusion and Future Works

7.1 Conclusions

Multi-building hierarchical control for the integration of prosumers in the electrical network has been modelled and simulated in this thesis. The simulated results verify the theory about hierarchical control of microgrid applied to multi-building microgrid. An improved secondary controller with Smith Predictor has been proposed, which improves the microgrid stability. This proposed secondary controller has been simulated with adverse communication delay condition to check its validity. The system is proven to be robust backed by simulation results. Communication outage is also covered in one of the sections, the microgrid being robust enough to support this kind of contingencies. Improved methods regarding communication failure is suggested for further works. A simplified tertiary control has been modelled to find control parameters. The presented complete model of the tertiary control is based on existing techniques for its application in the microgrid under study. Although the results are promising, the tertiary control performance still needs for improvements. Some possible improvements regarding the tertiary control are proposed as future work.

7.2 Future works

The present work has led to several lines of study and room for improvement in the hierarchical control of microgrids, the main suggested future lines are the following:

1. Modelled simulations can be improved and the use of hardware in the loop and real time simulations can be explored given the complexity of the studied system.

2. Instead of centralized secondary control, a decentralized secondary control architecture could be used. This allows the control of voltage and frequency at the building node. Thus, appropriate control signals will be locally sent to the primary controller of the other buildings. In this way, the failure of a building communication channel will only fail down that individual building and other buildings can work independently. Thus, adding more buildings in the MG will be easy, making the system expandable. The advantage of this architecture is that the communication system is not too busy, since only unidirectional messages are sent in only one direction.

3. The future developments can consider the introduction of the inner loops and the behavior of the power converters in the system simulation. As an alternative to the commonly used grid-supporting based on droop control, the use of virtual synchronous generators (VSG) is suggested for future developments.

4. Tertiary control response may be improved by feed-forwarding the power references inside the buildings to reduce the coupling effect.

Appendix A

Parameter Tables

Table A.1: General Simulation Parameters

General Parameters	Symbol	Value
Nominal Frequency	f_0	50Hz
Nominal Voltage	V_0	326.6V
Sampling Time	T_s	0.0001s
Communication Delay	T_{delay}	1s

Table A.2: Primary Droop Control Parameters

Primary Droop Control Parameters	Symbol	Value
Maximum Active Power	P_{max}	100kW
Maximum Reactive Power	Q_{max}	100kVAr
Nominal Active Power	P_0	0kW
Nominal Reactive Power	Q_0	0kVAr
Minimum Allowable Voltage	f_{min}	292.7V
Maximum Allowable Voltage	V_{max}	357.7
Minimum Allowable Frequency	V_{min}	48Hz
Active Power Droop Coefficient	C_P	2e-05
Reactive Power Droop Coefficient	C_Q	3.2527e-04

Table A.3: Secondary Control Parameters

Secondary Control Parameter	Symbol	Value
Proportional Gain without Smith Predictor f and V	G_{pf},G_{pv}	0.0001
Integral Gain without Smith Predictor f and V	G_{if},G_{iv}	1750
Proportional Gain with Smith Predictor f and V	G_{pf},G_{pv}	0.0005
Integral Gain with Smith Predictor f and V	G_{if},G_{iv}	5000
Voltage Saturation	V_{sat}	$\pm120V$
Frequency Saturation	f_{sat}	$\pm10Hz$

Table A.4: Tertiary Control Parameters

Tertiary Control Parameters	Symbol	Value
Simplified Model Proportional Gain P and Q	G_{pP},G_{pQ}	1.025e-06,0.00642
Simplified Model Integral Gain P and Q	G_{iP},G_{iQ}	0.1335,7.5
Original Model Proportional Gain P and Q	G_{pP},G_{pQ}	2.2e-5,0.16
Original Model Integral Gain P and Q	G_{iP},G_{iQ}	1.6e-7,4227

Table A.5: Line Impedance Parameters

Line Impedance Parameters	Symbol	Value
Resistance	R_{line}	0.642
X/R ratio	X/R	0.32
Inductance	L_{line}	0.6539

Table A.6: Grid Impedance Parameters

Grid Impedance Parameters	Symbol	Value
Resistance Grid	R_{grid}	6.42
Inductance Grid	L_{grid}	0.0065

Appendix B

Simulink Figures

Figure B-1: Primary droop control(local controller).

Frequency Droop

Voltage Droop

PB1 → +_ → Kgd → f0 +_ → +_ → 2 Con_f

del_f_B1

P0 P0

QB1 → +_ → Kad → -C- U0 → +_ → +_ → 1 Con_V

del_V_B1

Q0 Q0

2*pi → (K Ts)/(z-1) → sin / cos → -T-

v_abc_bus_g_1 → Vabc P → PB1

_abc_bus_g_1 → Iabc Q → QB1
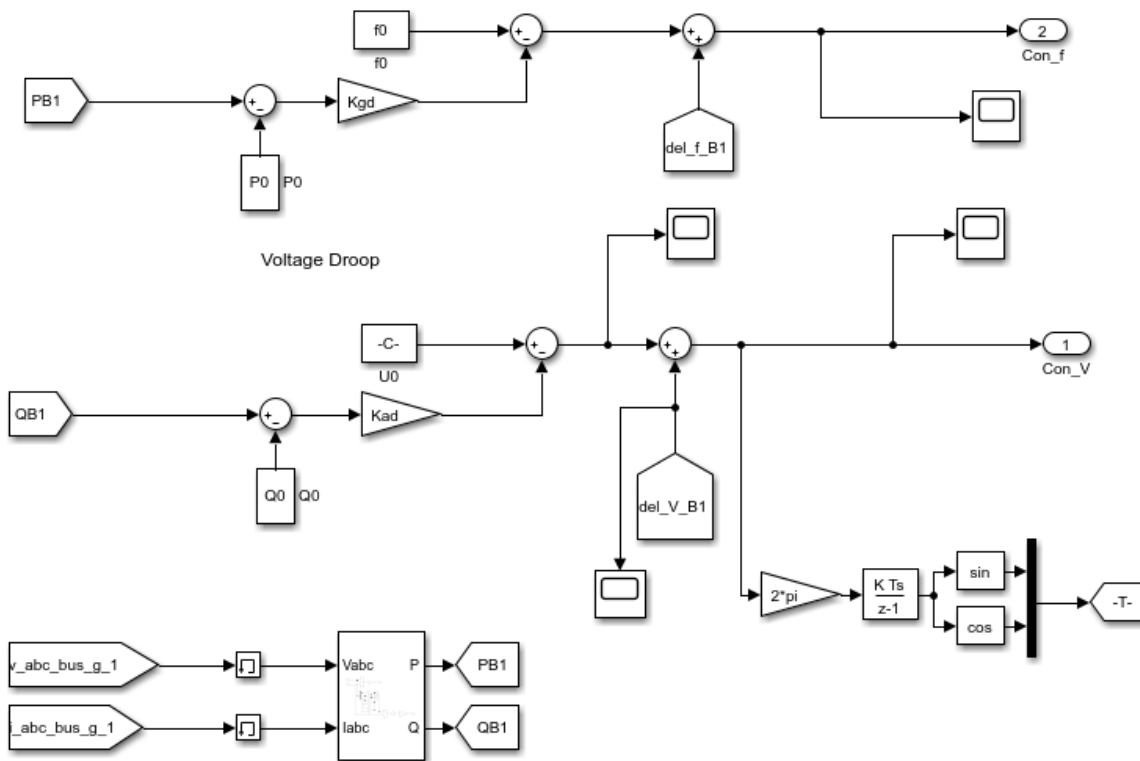
Figure B-2: Model of grid-forming converter
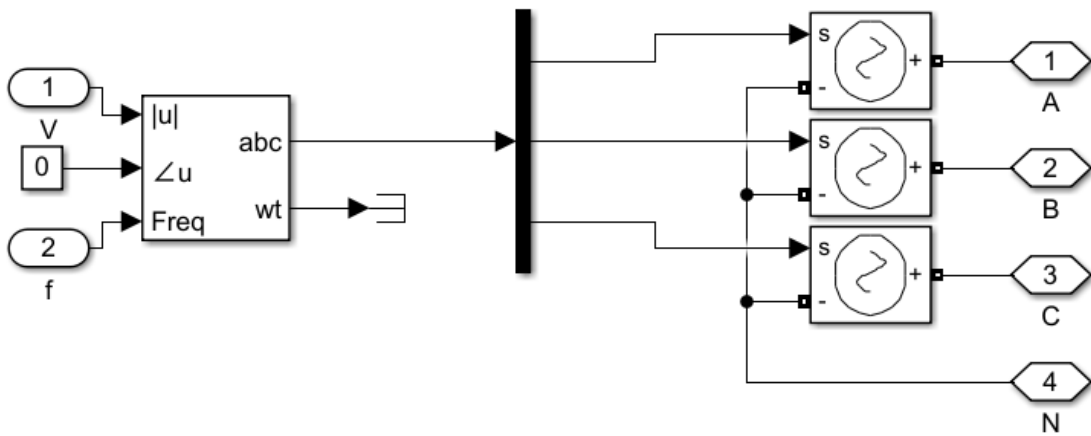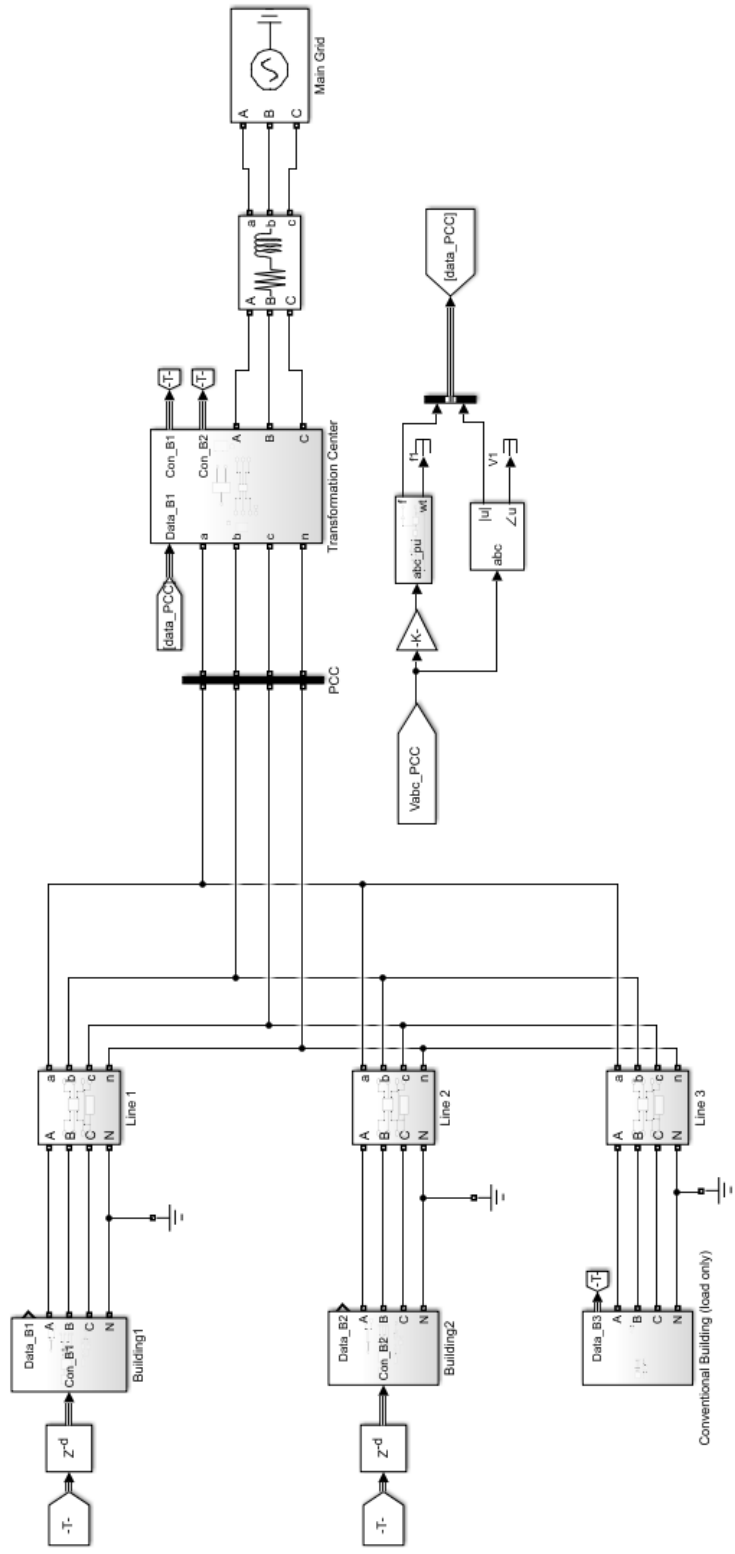
Figure B-3: Simulink model of multi-building MG understudy.

Figure B-4: Secondary controller in DHEMS building 1.
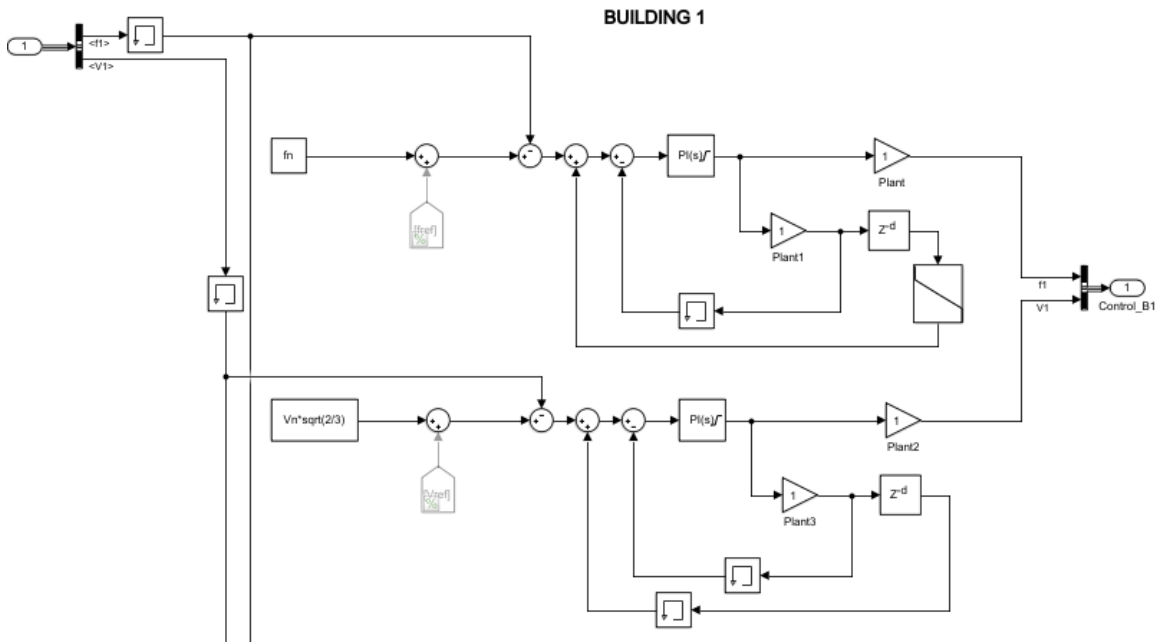
Figure B-5: Secondary controller in DHEMS building 2.
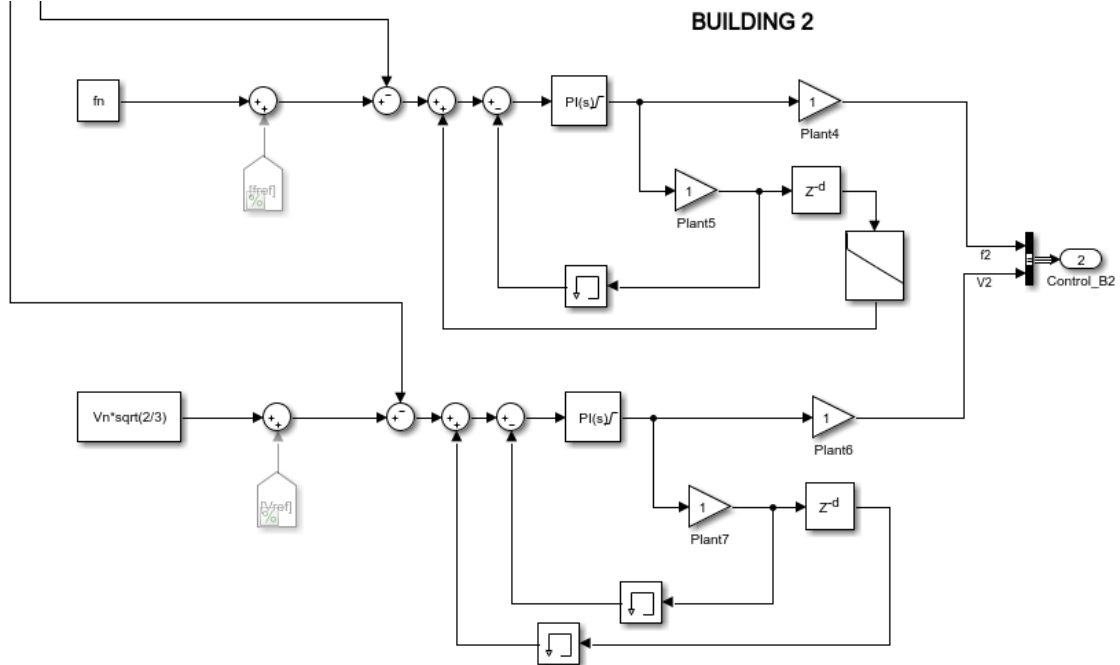
Figure B-6: Synchronization implementation of microgrid to the main grid.
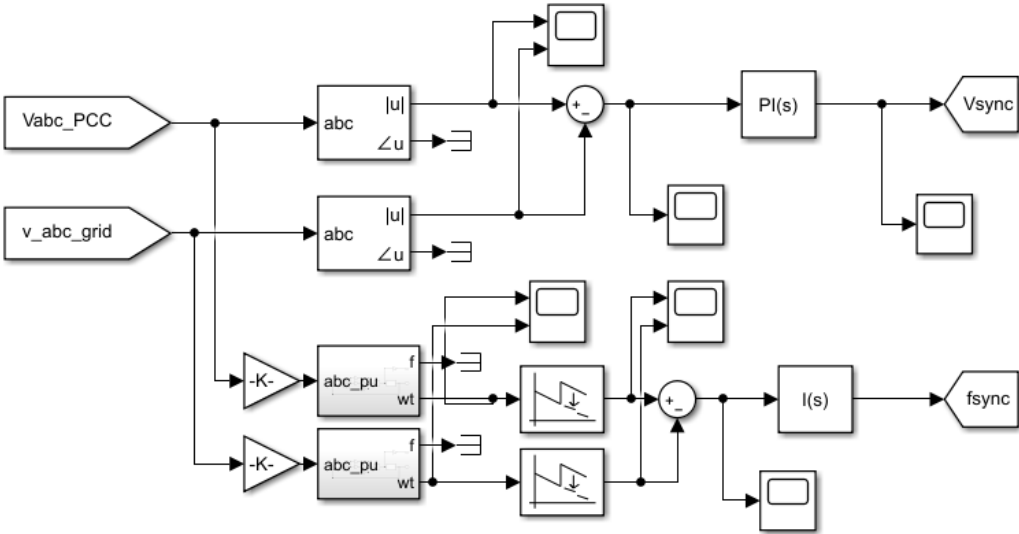
Figure B-7: Tertiary controller.
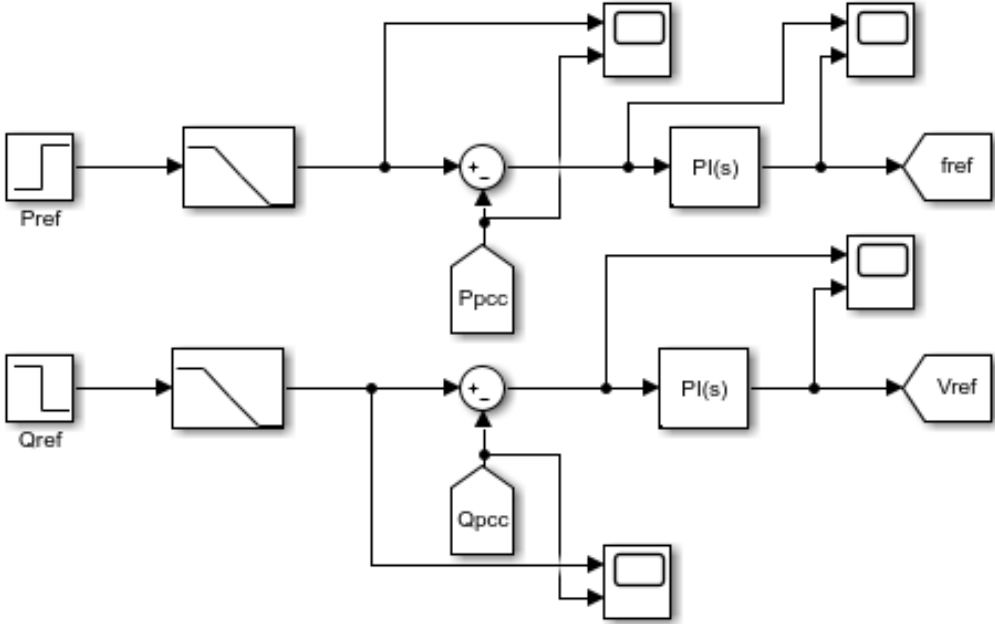
Figure B-8: Simplified model of voltage secondary control
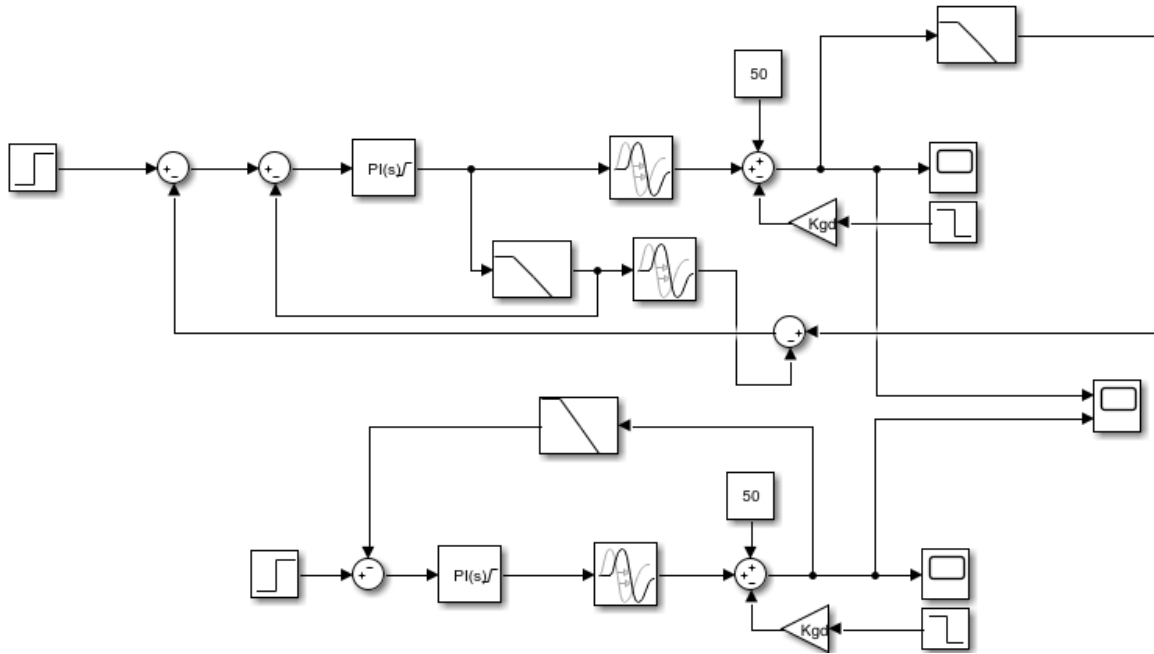
Figure B-9: Simplified model of frequency secondary control
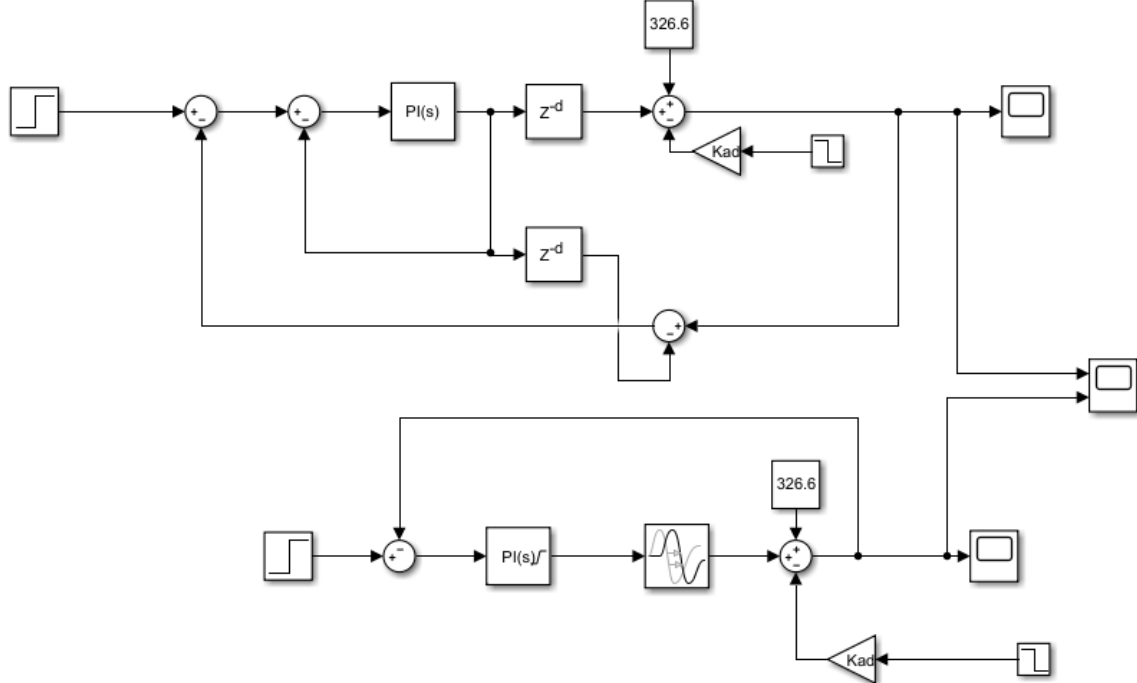
Bibliography

[1] A. Bidram and A. Davoudi, "Hierarchical structure of microgrids control system," *IEEE Transactions on Smart Grid*, vol. 3, no. 4, pp. 1963–1976, 2012.

[2] J. Rocabert, A. Luna, F. Blaabjerg, and P. Rodriguez, "Control of power converters in ac microgrids," *IEEE transactions on power electronics*, vol. 27, no. 11, pp. 4734–4749, 2012.

[3] J. W. Simpson-Porco, F. Dörfler, F. Bullo, Q. Shafiee, and J. M. Guerrero, "Stability, power sharing, & distributed secondary control in droop-controlled microgrids," in *2013 IEEE International Conference on Smart Grid Communications (SmartGridComm)*, pp. 672–677, IEEE, 2013.

[4] J. M. Guerrero, M. Chandorkar, T.-L. Lee, and P. C. Loh, "Advanced control architectures for intelligent microgrids—part i: Decentralized and hierarchical control," *IEEE Transactions on Industrial Electronics*, vol. 60, no. 4, pp. 1254–1262, 2012.

[5] O. Palizban and K. Kauhaniemi, "Hierarchical control structure in microgrids with distributed generation: Island and grid-connected mode," *Renewable and Sustainable Energy Reviews*, vol. 44, pp. 797–813, 2015.

[6] A. Mirzal, "Delay compensation using the smith predictor: a brief review with numerical examples," *International Journal of Computer-aided Mechanical Design and Implementation*, vol. 3, no. 1, pp. 1–8, 2017.

[7] J. C. Vasquez, J. M. Guerrero, M. Savaghebi, J. Eloy-Garcia, and R. Teodorescu, "Modeling, analysis, and design of stationary-reference-frame droop-controlled parallel three-phase voltage source inverters," *IEEE Transactions on Industrial Electronics*, vol. 60, no. 4, pp. 1271–1280, 2012.

[8] R. H. Lasseter, "Microgrids," in *2002 IEEE Power Engineering Society Winter Meeting. Conference Proceedings (Cat. No. 02CH37309)*, vol. 1, pp. 305–308, IEEE, 2002.

[9] J. W. Simpson-Porco, Q. Shafiee, F. Dörfler, J. C. Vasquez, J. M. Guerrero, and F. Bullo, "Secondary frequency and voltage control of islanded microgrids via distributed averaging," *IEEE Transactions on Industrial Electronics*, vol. 62, no. 11, pp. 7025–7038, 2015.

[10] J. M. Guerrero, J. C. Vasquez, J. Matas, L. G. De Vicuña, and M. Castilla, "Hierarchical control of droop-controlled ac and dc microgrids—a general approach toward standardization," *IEEE Transactions on industrial electronics*, vol. 58, no. 1, pp. 158–172, 2010.

[11] J. M. Guerrero, P. C. Loh, T.-L. Lee, and M. Chandorkar, "Advanced control architectures for intelligent microgrids—part ii: Power quality, energy storage, and ac/dc microgrids," *IEEE Transactions on industrial electronics*, vol. 60, no. 4, pp. 1263–1270, 2012.

[12] A. Mohd, E. Ortjohann, D. Morton, and O. Omari, "Review of control techniques for inverters parallel operation," *Electric Power Systems Research*, vol. 80, no. 12, pp. 1477–1487, 2010.

[13] J. P. Lopes, C. Moreira, and A. Madureira, "Defining control strategies for microgrids islanded operation," *IEEE Transactions on power systems*, vol. 21, no. 2, pp. 916–924, 2006.

[14] Q. Shafiee, J. M. Guerrero, and J. C. Vasquez, "Distributed secondary control for islanded microgrids—a novel approach," *IEEE Transactions on power electronics*, vol. 29, no. 2, pp. 1018–1031, 2013.

[15] S. Milčiuvienė, J. Kiršienė, E. Doheijo, R. Urbonas, and D. Milčius, "The role of renewable energy prosumers in implementing energy justice theory," *Sustainability*, vol. 11, no. 19, p. 5286, 2019.

[16] H. Nikkhajoei and R. H. Lasseter, "Distributed generation interface to the certs microgrid," *IEEE transactions on power delivery*, vol. 24, no. 3, pp. 1598–1608, 2009.

[17] A. Madureira, C. Moreira, and J. P. Lopes, "Secondary load-frequency control for microgrids in islanded operation," in *Proc. Int. Conf. Renewable Energy Power Quality*, 2005.

[18] A. Micallef, M. Apap, C. Spiteri-Staines, and J. M. Guerrero, "Secondary control for reactive power sharing in droop-controlled islanded microgrids," in *2012 IEEE International Symposium on Industrial Electronics*, pp. 1627–1633, IEEE, 2012.

[19] Y. Zhang and H. Ma, "Theoretical and experimental investigation of networked control for parallel operation of inverters," *IEEE Transactions on Industrial Electronics*, vol. 59, no. 4, pp. 1961–1970, 2011.

[20] H. Laaksonen, P. Saari, and R. Komulainen, "Voltage and frequency control of inverter based weak lv network microgrid," in *2005 International Conference on Future Power Systems*, pp. 6–pp, IEEE, 2005.

[21] K. De Brabandere, "Voltage and frequency droop control in low voltage grids by distributed generators with inverter front-end (spannings-en frequentieregeling in

laagspanningsnetten door gedistribueerde opwekkers met vermogenelektronische netkoppeling),” 2006.

[22] J. M. Guerrero, J. Matas, L. G. D. V. De Vicuna, M. Castilla, and J. Miret, “Wireless-control strategy for parallel operation of distributed-generation inverters,” *IEEE Transactions on Industrial Electronics*, vol. 53, no. 5, pp. 1461–1470, 2006.

[23] Z. Ye, A. Kolwalkar, Y. Zhang, P. Du, and R. Walling, “Evaluation of anti-islanding schemes based on nondetection zone concept,” *IEEE transactions on power electronics*, vol. 19, no. 5, pp. 1171–1176, 2004.

[24] M. Liserre, A. Pigazo, A. Dell'Aquila, and V. M. Moreno, “An anti-islanding method for single-phase inverters based on a grid voltage sensorless control,” *IEEE Transactions on Industrial Electronics*, vol. 53, no. 5, pp. 1418–1426, 2006.

[25] H. Zeineldin, E. El-Saadany, and M. Salama, “Distributed generation microgrid operation: Control and protection,” in *2006 Power Systems Conference: Advanced Metering, Protection, Control, Communication, and Distributed Resources*, pp. 105–111, IEEE, 2006.

[26] H. H. Zeineldin, “A q–f droop curve for facilitating islanding detection of inverter-based distributed generation,” *IEEE transactions on power electronics*, vol. 24, no. 3, pp. 665–673, 2009.

[27] G. Chen and E. Feng, “Distributed secondary control and optimal power sharing in microgrids,” *IEEE/CAA Journal of Automatica Sinica*, vol. 2, no. 3, pp. 304–312, 2015.

[28] M. C. Chandorkar, D. M. Divan, and R. Adapa, “Control of parallel connected inverters in standalone ac supply systems,” *IEEE transactions on industry applications*, vol. 29, no. 1, pp. 136–143, 1993.

[29] A. O'Dwyer, *The estimation and compensation of processes with time delays*. PhD thesis, Dublin City University, 1996.

[30] G. F. Frankin, J. D. Powell, and A. Emami-Naeini, “Feedback control of dynamic systems,” *Reading, MA: Addison-Wesley*, vol. 10, pp. 20–30, 1994.

[31] A. O'Dwyer, “Performance and robustness issues in the compensation of folpd processes with pi and pid controllers,” 1998.

[32] G. Stephanopoulos, *Chemical process control*, vol. 2. Prentice hall New Jersey, 1984.

[33] C. Zhang, J. Wu, Y. Zhou, M. Cheng, and C. Long, “Peer-to-peer energy trading in a microgrid,” *Applied Energy*, vol. 220, pp. 1–12, 2018.